HHS Public Access

Author manuscript

Nat Med. Author manuscript; available in PMC 2014 May 01.

Published in final edited form as:

Nat Med. 2013 November ; 19(11): 1478–1488. doi:10.1038/nm.3322.

Mst1 inhibits autophagy by promoting Beclin1-Bcl-2 interaction

Yasuhiro Maejima[1,4], **Shiori Kyoi**[1], **Peiyong Zhai**[1], **Tong Liu**[2], **Hong Li**[2], **Andreas Ivessa**[1], **Sebastiano Sciarretta**[1], **Dominic P. Del Re**[1], **Daniela K. Zablocki**[1], **Chiao-Po Hsu**[3], **Dae-Sik Lim**[5], **Mitsuaki Isobe**[4], and **Junichi Sadoshima**[1,6]

[1]Cardiovascular Research Institute, Department of Cell Biology and Molecular Medicine, Rutgers, The State University of New Jersey, New Jersey Medical School, Newark, NJ 07103

[2]Center for Advanced Proteomics Research and Department of Biochemistry and Molecular Biology, Rutgers, The State University of New Jersey, New Jersey Medical School, Newark, NJ 07103

[3]Division of Cardiovascular Surgery, Department of Surgery, Taipei Veterans General Hospital, National Yang-Ming University School of Medicine, Taipei, Taiwan, Republic of China

[4]Department of Cardiovascular Medicine, Tokyo Medical and Dental University, Tokyo, 113-8519, Japan

[5]Creative Research Center of Cell Division and Differentiation, Department of Biological Sciences, KAIST, Daejeon, 305-701, Republic of Korea

Here we show that Mammalian Ste20-like kinase 1 (Mst1), a pro-apoptotic kinase, negatively regulates protein quality control mechanisms through inhibition of autophagy in the heart. Stress-induced activation of Mst1 promotes accumulation of p62/SQSTM1 and aggresome formation, which are accompanied by the disappearance of autophagosomes in cardiomyocytes. Mst1 phosphorylates threonine 108 in the BH3 domain of Beclin1, which enhances interaction between Beclin1 and Bcl-2/Bcl-xL, stabilizes the Beclin1 homodimer, inhibits the PI3 kinase activity of the Atg14L-Beclin1-Vps34 complex, and suppresses autophagy. Furthermore, Mst1-induced sequestration of Bcl-2/Bcl-xL by Beclin1 allows Bax to become active, thereby stimulating apoptosis. Increased Mst1 activity is associated with cardiac dysfunction after myocardial infarction and dilated cardiomyopathy, due to inhibition of autophagy and aggresome accumulation. These results suggest that Mst1 coordinately regulates autophagy and apoptosis through phosphorylation of Beclin1 and consequent modulation of a three-way interaction between the Bcl-2 proteins, Beclin1 and Bax.

[6]Address correspondence to: Junichi Sadoshima MD PhD, Cardiovascular Research Institute, Department of Cell Biology and Molecular Medicine, Rutgers, The State University of New Jersey, New Jersey Medical School, 185 South Orange Ave, MSB G-609, Newark, NJ 07103, sadoshju@umdnj.edu, Phone (973) 972-8619, Fax (973) 972-8919.

Author Contributions

Y.M. designed and performed experiments, analyzed data and wrote the manuscript. S.K. designed and performed experiments and analyzed data. P.Z. performed animal surgery. T.L. and H.L. performed experiments and analyzed data regarding proteomic analyses. A.I., S.S, D.D., and C.H. performed experiments and analyzed data. D.Z. wrote the manuscript. D.L. provided the animals and cells, and supervised the project. M.I. supervised the project. J.S. designed the studies, analyzed the data and wrote the manuscript.

Autophagy is a bulk degradation mechanism in which cytosolic proteins and organelles are sequestrated into autophagosomes and degraded by lysosomes [1]. Due to its large capacity, autophagy plays an essential role in maintaining organelle functions and protein quality by removing damaged organelles and protein aggregates. Suppression of autophagy below physiological levels through genetic deletion of Atg5 induces heart failure with enhanced protein aggregation, suggesting that autophagy is required to maintain baseline heart function [2]. Autophagy is upregulated in various pathological conditions, including myocardial ischemia, ischemia/reperfusion (I/R), and pressure overload [3–5]. Upregulation of autophagy during myocardial stress is generally compensatory, alleviating energy loss and scavenging damaged mitochondria and protein aggregates [3, 6]. On the other hand, deregulated activation of autophagy leads to excessive self-digestion and eventual cell death. I/R markedly upregulates Beclin1 and stimulates massive autophagy in the heart, and suppression of autophagy by downregulation of Beclin1 attenuates myocardial injury [4]. A possible explanation for the dichotomous function of autophagy in the heart is that autophagic activity either above or below the physiological range is detrimental [7, 8]. Currently, however, the signaling mechanism responsible for maintaining autophagic activity within the proper range is poorly understood.

Beclin1, a Bcl-2-homology (BH)-3 domain-only protein [9], plays an important role in both autophagosome formation and autolysosome fusion. Beclin1 and the class III-type phosphoinositide 3-kinase (Class III PI3K/Vps34) form two distinct complexes [10]. In complex I, which mediates autophagosome formation, Atg14L bridges between Beclin1 and the Vps34-p150 complex, whereas in complex II, which regulates the vacuolar protein sorting pathway, UVRAG bridges between Beclin1 and the Vps34-p150 complex [11]. The kinase activity of the Beclin1-Vps34 complex is negatively regulated by Bcl-2 family proteins [12], which bind to Beclin1 and disrupt the interaction between Beclin1 and Vps34, thereby inhibiting autophagosome formation [7]. However, it remains unclear how Beclin1 and Bcl-2 family proteins associate with one another and induce formation of the inactive Beclin1 homodimer at baseline.

Mammalian sterile 20-like kinase 1 (Mst1) is a serine threonine kinase and a component of the "*Hippo*" signaling pathway, which regulates apoptosis and organ size [13]. Mst1 is one of the protein kinases most strongly activated during cardiomyocyte apoptosis [14], through either a Ras associated domain family 1 isoform A (Rassf1A)-dependent [15] or a caspase-dependent mechanism [14–16]. Persistent Mst1 activation in the heart induces dilated cardiomyopathy (DCM), whereas inhibition of endogenous Mst1 prevents apoptosis and cardiomyopathy in response to pathologically relevant stresses [14, 16]. Mst1 facilitates accumulation of protein aggresomes and p62/SQSTM1 in the heart *in vivo* (Fig. 2a,b and Supplementary Fig. 1e,f). This led us to hypothesize that Mst1 activation in response to stress inhibits autophagy, detrimentally affecting cardiomyocytes (CMs) and promoting heart failure.

Thus, the goals in this study were 1) to examine whether Mst1 inhibits autophagy in the heart, and, if so, 2) to examine the molecular mechanism by which Mst1 regulates the autophagic machinery, and, finally, 3) to show that Mst1-induced suppression of autophagy

is involved in protein aggresome accumulation and cardiac dysfunction during cardiac remodeling.

Results

Endogenous Mst1 promotes cardiac dysfunction through inhibition of autophagy after myocardial infarction (MI)

We previously showed that endogenous Mst1 plays an essential role in mediating left ventricular (LV) dysfunction after MI [16]. Heart failure is often accompanied by accumulation of damaged proteins and organelles, in the form of aggresomes. Microscopic analyses of the chronic MI mouse heart showed that aggresomes accumulate in the perinucleus of border zone and remote area CMs (Fig. 1a). The aggresomes co-localized with p62/SQSTM1 (p62), a protein known to be degraded by autophagy, suggesting insufficient clearance of aggresomes by autophagy (Fig. 1a). The accumulation of aggresomes and p62 was markedly attenuated in transgenic mice with cardiac-specific overexpression of DN-Mst1 (Tg-DN-Mst1) and *Mst1*$^{-/-}$ mice, suggesting that endogenous Mst1 negatively affects protein and organelle quality control in post MI hearts (Fig. 1a). Autophagy is activated in the post MI heart, as evidenced by increases in LC3-II (Fig. 1b) and accumulation of GFP-LC3 puncta in the border zone in transgenic mice harboring GFP-LC3 (Tg-GFP-LC3) (Fig. 1c). Suppression of Mst1 enhanced the indicators of autophagy in the post MI hearts, suggesting that endogenous Mst1 negatively regulates autophagy (Fig. 1b,c). In order to elucidate the role of autophagy in mediating the protection observed in Tg-DN-Mst1 mice [16], we crossed Tg-DN-Mst1 mice with *Beclin1*$^{+/-}$ mice. The reduction in both protein aggregation and p62 accumulation observed in Tg-DN-Mst1 mice was reversed and the increase in GFP-LC3 puncta was suppressed in the *Beclin1*$^{+/-}$-Tg-DN-Mst1 hearts, indicating suppression of autophagy (Fig. 1a – c and Supplementary Fig. 1a). Furthermore, the suppression of LV remodeling, MI scar contraction, and improved LV function and survival rate observed in Tg-DN-Mst1 mice were all reversed in the *Beclin1*$^{+/-}$-Tg-DN-Mst1 mouse hearts (Fig. 1d,e and Supplementary Fig. 1b – d). These results suggest that autophagy plays an important role in mediating the protective effects of Mst1 suppression in the post MI heart.

Mst1 promotes protein aggregate accumulation in cardiomyocytes

We examined whether Mst1 activation is sufficient to induce aggresome formation. Cardiac-specific Mst1 transgenic mice (Tg-Mst1) exhibited more polyubiquitinated protein (Fig. 2a and Supplementary Fig. 1e) and stronger co-localization of vimentin and αB-crystallin in the perinucleus of CMs than non-transgenic (NTg) mice (Supplementary Fig. 1f). Co-localization of aggresomes and p62 was markedly greater in Tg-Mst1 than in NTg (Fig. 2b). Increased co-localization of aggresomes and p62 was also observed in CMs overexpressing Mst1 (Fig. 2c and Supplementary Fig. 1g), indicating a cell autonomous effect. Using transmission electron microscopy (TEM), electron-dense amorphous structures characteristically consistent with aggresomes [17] were observed in Tg-Mst1 CMs (Fig. 2d and Supplementary Fig. 1h). These results suggest that Mst1 activation is sufficient to stimulate protein aggregation. Mst1 suppressed long-lived protein degradation compared to LacZ in CMs. Conversely, transduction with adenovirus harboring DN-Mst1 (Ad-DN-Mst1)

or knockdown of Mst1 by an adenovirus harboring shRNA for Mst1 (Ad-sh-Mst1) increased long-lived protein degradation under both nutrient-rich and starved conditions (Fig. 2e). We then investigated the effect of Mst1-induced aggresome accumulation upon CM survival independently of the pro-apoptotic effect of Mst1. Although the increase in cell death induced by Mst1 overexpression was suppressed by zVAD-fmk, a pan-caspase inhibitor, during the initial 48 hours of Mst1 transduction, Mst1 still induced cell death after 72 hours of transduction, accompanied by aggresome formation (Supplementary Fig 1i). Thus, Mst1 erodes protein quality control, thereby promoting cell death in CMs.

Mst1 negatively regulates autophagy in cardiomyocytes

Autophagosomes, observed by TEM, and GFP-LC3 puncta were significantly fewer in Tg-Mst1 than in NTg mice at baseline, and remained fewer even after starvation. Conversely, there were significantly more autophagosomes in Tg-DN-Mst1 and *Mst1*$^{-/-}$ than in NTg mice both at baseline and after starvation (Fig. 2f and Supplementary Fig. 2a,b). There was significantly less LC3-II and significantly more p62 in Tg-Mst1 than in NTg hearts. Conversely, there was significantly more LC3-II and significantly less p62 in Tg-DN-Mst1 and *Mst1*$^{-/-}$ than in NTg hearts (Fig. 2g and Supplementary Fig. 2c). These results suggest that Mst1 negatively regulates autophagy. Mst1 significantly inhibited accumulation of GFP-LC3 puncta in the presence of chloroquine (Cq, 10 mg kg^{-1}, ip injection), an inhibitor of autophagosome-lysosome fusion [18] (Supplementary Fig. 2d). In CMs transduced with Ad-mRFP-GFP-LC3 [19], Mst1 significantly decreased the number of both green and red puncta compared to LacZ, and there was a significantly smaller increase in the number of red puncta, corresponding to autolysosomes, than yellow puncta, corresponding to autophagosomes, in merged images. Conversely, knockdown of Mst1 significantly increased the number of both green and red puncta compared to LacZ, and there was a significantly greater increase in the number of red puncta than yellow puncta in merged images (Fig. 2h and Supplementary Fig. 2e). These results suggest that Mst1 inhibits autophagic flux. Mst1 also potently inhibited both baseline and GD-induced autophagy in CMs, as evidenced by a decrease in LC3-II, an increase in p62, and a decrease in the number of GFP-LC3 puncta, whereas inhibition of endogenous Mst1 stimulated autophagy, suggesting that Mst1 suppression of autophagy is cell-autonomous (Supplementary Fig. 2f,g). WW45 downregulation moderately promoted autophagy but increased Lats2 expression did not modulate autophagy (Supplementary Fig. 2h), suggesting that components of the *Hippo* pathway upstream of Mst1 negatively affect autophagy through Mst1 but those downstream of Mst1 may not. GD-induced autophagy was also enhanced in *Mst1*$^{-/-}$- and *Mst1*$^{-/-}$ *Mst2*$^{-/-}$-MEFs compared to in WT-MEFs (Supplementary Fig. 2i,j), suggesting that Mst1 suppression of autophagy also functions in other cell types.

Mst1 physically interacts with Beclin1, thereby inhibiting the Beclin1-Vps34 complex

In order to elucidate how Mst1 inhibits autophagy, we investigated whether Mst1 interacts with autophagy-associated proteins, including ULK1, Atg4B, Atg5, Beclin1, Atg7, and LC3, in CMs using co-immunoprecipitation assays. Endogenous Beclin1 strongly interacted with Mst1 both *in vitro* and *in vivo*, while ULK1, a homolog of yeast Atg1, only weakly interacted with Mst1 *in vitro* (Fig. 3a and Supplementary Fig. 3a,b). None of the other autophagy-associated proteins interacted with Mst1. Mst1 significantly decreased Vps34

lipid kinase activity in CMs (Supplementary Fig. 3c). The activity of Atg14L-associated Vps34, reflecting complex I activity [10, 11], was also significantly suppressed in the presence of Mst1 (Fig. 3b). The number of GFP-2xFYVE dots, indicating *in situ* activity of the Beclin1-Vps34 complex [20], was also significantly decreased in the presence of Mst1, but was increased by inhibition of endogenous Mst1 (Fig. 3c), suggesting that Mst1 negatively regulates Beclin1-Vps34 complex activity. Mst1 significantly attenuated the interactions between Beclin1 and Vps34 and between Beclin1 and Atg14L (Fig. 3d), suggesting that Mst1 induces dissociation of complex I.

Complex I activity is modulated by several Beclin1-interacting proteins. We evaluated whether Mst1 affects interaction between Beclin1 and Bcl-2, Bcl-xL, Rubicon, Atg14L or UVRAG using co-immunoprecipitation assays in CMs. Mst1 significantly enhanced binding of both Bcl-2 and Bcl-xL to Beclin1 but attenuated Atg14L binding to Beclin1, both *in vitro* and *in vivo* (Fig. 3e and 3f). Neither Rubicon nor UVRAG binding to Beclin1 was affected by Mst1. The binding of Beclin1 to Atg14L was significantly increased and the binding of Bcl-2/Bcl-xL to Beclin1 was markedly attenuated in Tg-DN-Mst1 and *Mst1*$^{-/-}$ mouse hearts (Fig. 3f and Supplementary Fig. 3d), suggesting that Mst1 is a physiological kinase mediating the interaction between Beclin1 and Bcl-2/Bcl-xL, molecules known to disrupt the interaction between Beclin1 and Vps34. Mst1 suppression of autophagy was abolished when Bcl-2 and Bcl-xL were downregulated (Fig. 3g and Supplementary Fig. 3e). Mst1 inhibition of autophagy was dose-dependently reversed by treatment with ABT-737 (Fig. 3h and Supplementary Fig. 3f), a BH3 mimetic [21] that significantly decreased the Mst1-induced increase in Bcl-2 binding to Beclin1 (Supplementary Fig. 3g). These results suggest that Mst1 inhibition of autophagy is mediated by interaction between Bcl-2/Bcl-xL and the BH3 domain of Beclin1.

Beclin1 associates with Atg14L when autophagy is stimulated but homodimerizes when inactive [22, 23]. Co-immunoprecipitation assays showed that Mst1 stimulated association between Flag-tagged Beclin1 and HA-tagged Beclin1 (Fig. 3i), suggesting that Mst1 inhibits interaction between Beclin1 and complex I by promoting formation of the inactive Beclin1 homodimer [22–25].

Mst1 phosphorylates Beclin1 at Thr^{108} in the BH3 domain

In vitro kinase assays showed that GST-Beclin1-WT containing full length Beclin1 and a Beclin1 fragment containing amino acids (AA) [72–163] (Beclin1-N2), but not other fragments, can be phosphorylated by Mst1 (Fig. 4a,b and Supplementary Fig. 4a). Using mass spectrometry, the threonine residue at position 108 (Thr^{108}) in Beclin1, located in the BH3 domain and highly conserved across species, was found to be phosphorylated by Mst1 (Fig. 4c and Supplementary Fig. 4b). GST-Beclin1 Thr108Ala (T108A) was not phosphorylated by Mst1 (Supplementary Fig. 4c), suggesting that Thr^{108} is the major site of phosphorylation by Mst1. Immunoblot analyses with phosphorylated Thr^{108}-specific antibody showed increased phosphorylated Beclin1 levels in the presence of Mst1, but not in the presence of DN-Mst1, in CMs *in vivo* and *in vitro* (Fig. 4d). Thr^{108}-phosphorylated Beclin1 accumulated significantly more in the perinucleus of CMs in Tg-Mst1 mice than in NTg mice (Fig. 4e). Thr^{108}-phosphorylated Beclin1 (Supplementary Fig. 4d) co-localized

with KDEL, a marker of the endoplasmic reticulum (ER), but not with TGN46, a marker of the Golgi apparatus, or with Mitotracker®, a mitochondrial marker (Fig. 4f and Supplementary Fig. 4e) in CMs, suggesting that Mst1 phosphorylates Thr^{108} of Beclin1 located in the ER.

Mst1-induced phosphorylation induces homodimerization of Beclin1

Interaction between GST-Beclin1-WT and Bcl-2 was enhanced when GST-Beclin1-WT was phosphorylated by Mst1 (Fig. 5a). GST-Beclin1 Thr108Asp (T108D), a phospho-mimetic mutant, interacted with both Bcl-2 and Bcl-xL to the same extent as GST-Beclin1-WT phosphorylated by Mst1, but GST-Beclin1-T108A was less able to interact with Bcl-2/Bcl-xL than GST-Beclin1-WT, even after a kinase reaction with Mst1 (Fig. 5b). Phosphorylation of GST-Beclin1-WT by Death-associated protein kinase (DAPK) decreased the interaction between GST-Beclin1-WT and Bcl-2 (Fig. 5a), as shown previously [26], confirming the specificity of our assay. These results suggest that Mst1 directly stimulates interaction between Beclin1 and Bcl-2. Crystal structure analysis of the Beclin1-Bcl-xL complex [27] revealed that Thr^{108} of Beclin1 is located in the N-terminus of the BH3 domain and interacts with the α3-helix of Bcl-xL at the entrance of the hydrophobic groove (Supplementary Fig. 5a,b). As His^{113} of Bcl-xL is a basic AA with a positive electric charge, phosphorylation of Thr^{108}, which confers a negative charge to Thr^{108}, should enhance its interaction with His^{113}. Consistent with our hypothesis, mutation of His^{117} of mouse Bcl-2, which corresponds to His^{113} of human Bcl-xL, to Ala dramatically decreased the interaction between GST-Beclin1-WT and Bcl-2, even in the presence of Mst1 (Fig. 5c).

In vitro binding assays using recombinant proteins showed that Bcl-2 interacts not only with GST-Beclin1-N2, which contains the BH3 domain, but also with GST-Beclin1-MID (AA [150–284]), which contains the coiled-coil domain (CCD). Mst1 kinase activity enhanced the interaction of Bcl-2 with GST-Beclin1-N2, but not GST-Beclin1-MID (Fig. 5d). GST-Beclin1-MID could not interact with truncated Bcl-2 missing the BH4 domain, suggesting that the Beclin1 CCD binds to Bcl-2 in its BH4 domain (Fig. 5e). Beclin1 homodimerization increased dramatically when Beclin1-WT was incubated with Bcl-2-WT after a kinase reaction with Mst1, but not in the absence of either Mst1 kinase activity or Bcl-2 (Fig. 5f and Supplementary Fig. 5c). These results suggest that phosphorylation of Beclin1 by Mst1 stabilizes Beclin1 homodimerization by enhancing interaction between Beclin1 and Bcl-2 (Supplementary Fig. 5d).

Mst1-induced phosphorylation of Beclin1 not only inhibits autophagy but also induces apoptosis by sequestering Bcl-2 from Bax

We investigated how Thr^{108} phosphorylation of Beclin1 affects autophagy. Beclin1-T108D suppressed the Vps34 kinase activity in the Atg14L-Beclin1 complex and significantly decreased the number of GFP-2xFYVE dots in *in situ* assays in CMs, even in the absence of Mst1. Conversely, Mst1 failed to suppress the Vps34 kinase activity or reduce the number of GFP-2xFYVE dots in the presence of Beclin1-T108A (Fig. 5g,h). The number of GFP-LC3 puncta in cultured CMs was increased in the presence of Beclin1-T108A at baseline (Fig. 6a). Under starved conditions, Beclin1-T108A abolished the Mst1-induced decrease in GFP-LC3 puncta. Conversely, Beclin1-T108D decreased the number of GFP-LC3 puncta in CMs

under starved conditions even in the absence of Mst1 overexpression. Similar results were obtained with immunoblot analyses (Supplementary Fig. 6a). These results suggest that Thr^{108} phosphorylation of Beclin1 by Mst1 negatively affects autophagy in CMs.

Since Bcl-2/Bcl-xL also bind to other BH3 domain-containing proteins, including Bax, altered interaction between Beclin1 and Bcl-2/Bcl-xL may affect Bax function. Bax knockdown significantly suppressed Mst1-induced apoptosis, suggesting that Mst1 stimulates CM apoptosis through Bax (Supplementary Fig. 6b). Consistently, Mst1 not only stimulated interaction between Beclin1 and Bcl-2 but also attenuated interaction between Bcl-2 and Bax, allowing Bax to take an active conformation. Beclin1-T108D also not only enhanced the interaction between Beclin1 and Bcl-2 but also decreased the interaction between Bax and Bcl-2 and increased the amount of active Bax even in the absence of Ad-Mst1. In contrast, Beclin1-T108A neither increased the interaction between Beclin1 and Bcl-2 nor decreased the interaction between Bax and Bcl-2, such that Bax remained inactive, even in the presence of Ad-Mst1 (Fig. 6b). Beclin1-T108D significantly increased the number of TUNEL-positive CMs and the amount of cleaved caspase-3, even in the absence of Ad-Mst1, whereas Beclin1-T108A suppressed the Mst1-induced increases in TUNEL-positive CMs and cleaved caspase-3 (Fig. 6c). Thus, an Mst1-induced increase in the interaction of Beclin1 with Bcl-2 family proteins not only inhibits autophagy but also enhances apoptosis through dissociation of Bcl-2 from Bax in CMs (Supplementary Fig. 6c).

Mst1 inhibited GD-induced autophagy and increased accumulation of aggresomes in $Bax^{-/-}Bak^{-/-}$-MEFs, as well as in WT-MEFs (Supplementary Fig 6d – f). Although knockdown of endogenous Bax and Bak significantly reduced Mst1-induced cell death during the initial 48 hours, Mst1 still decreased survival after 72 hours of Ad-Mst1 transduction compared to in Ad-LacZ-treated $Bax^{-/-}Bak^{-/-}$-MEFs (Supplementary Fig 6g). These results suggest that Mst1 promotes cell death independently of the Bax/Bak-mediated pathway by inhibiting autophagic activity and promoting protein aggregate accumulation.

Conversely, $Atg7^{-/-}$ MEFs with overexpressed Mst1 did not show additional perinuclear accumulation of aggresomes compared to Ad-LacZ-treated $Atg7^{-/-}$-MEFs (Supplementary Fig. 6h,i), suggesting that Atg7 downregulation and Mst1 impair protein quality control through a common mechanism. Mst1 transduction into $Atg7^{-/-}$-MEFs reduced survival after 48 and 72 hours compared to LacZ transduction, suggesting that the pro-apoptotic effect of Mst1 can kill MEFs independently of suppression of autophagy (Supplementary Fig. 6j).

Endogenous Mst1 plays an essential role in mediating phosphorylation of Beclin1 in the failing heart

We investigated whether Thr^{108} of Beclin1 is phosphorylated in the post MI heart. Six weeks after MI surgery, the Thr^{108}-phosphorylated Beclin1 level was significantly elevated in NTg hearts but not in Tg-DN-Mst1 or $Mst1^{-/-}$ hearts, suggesting that endogenous Mst1 phosphorylates Beclin1 in CMs in the post MI heart (Fig. 6d,e).

We here demonstrate that increased activation of Mst1 inhibits autophagy below the physiological level by promoting Beclin1-Bcl-2 interaction, thereby inducing chronic heart failure. On the other hand, we have also shown that excessive activation of autophagy

beyond a physiological range causes cell death, thereby aggravating cardiac function [4]. Beclin1 is strongly upregulated by I/R [4], but the protein level of Beclin1 gradually decreases in the chronic phase of MI. As the amount of endogenous Mst1 molecules is limited, even though the activity of Mst1 is upregulated during stress conditions (Supplementary Fig. 6k) [14], strong upregulation of Beclin1 should increase the amount of unphosphorylated Beclin1, as appears to be the case in I/R (Supplementary Fig. 6l), as well as subsequent activation of the Vps34 complex. In fact, experiments show that Beclin1 overexpression does alleviate Mst1-induced suppression of autophagy in CMs (Supplementary Fig. 6m). Thus, we propose that the extent of autophagy in the heart may be modulated by the balance between Mst1 activation and Beclin1 expression.

Finally, we investigated whether the Mst1-Beclin1 interaction-mediated detrimental effect is also present in human failing hearts. Mst1 activity and the amount of Thr^{108}-phosphorylated Beclin1 were significantly higher in failing hearts from individuals with end-stage DCM who received heart transplants than in hearts from donors with normal cardiac function (Fig. 6f and Supplementary Table 1). The amount of p62 was also significantly higher and the LC3-II amount was significantly lower in the failing hearts than in the normal hearts (Fig. 6f), suggesting that autophagy is suppressed in the failing human heart. Staining of myocardial sections showed more prominent co-localization of aggresomes with p62 in the perinucleus of CMs in the failing hearts than in normal hearts (Fig. 6g).

Discussion

A variety of disorders, collectively termed proteinopathies, are characterized by intracellular deposition of aggresomes, including neurodegenerative disorders, liver insufficiencies and heart failure caused by volume and pressure overload [28, 29]. Abnormalities in the protein degradation mechanisms, namely, the ubiquitin proteasome system and autophagy, can cause proteinopathies, but how they are regulated by the stress-signaling pathway is poorly understood. We here demonstrate that Mst1, a pro-apoptotic kinase, facilitates proteinopathy in a chronic MI model by directly inhibiting autophagy through phosphorylation of Beclin1, a key regulator of autophagosome formation. Mst1-induced phosphorylation of Beclin1 induces interdependent modulation of Beclin1, Bcl-2/Bcl-xL and Bax, thereby regulating autophagy and apoptosis simultaneously. Furthermore, Mst1 activation, Beclin1 phosphorylation, attenuation of autophagy and protein aggregate accumulation are all exacerbated in human end-stage DCM hearts. Thus, Mst1 may be an important target for treatment in heart failure patients.

Beclin1 physically interacts with the Bcl-2 family proteins, and their interaction can be modulated by phosphorylation, including phosphorylation of Beclin1 in the BH3 domain by DAPK and Bcl-2 in its nonstructural loop by JNK1, thereby promoting dissociation of Beclin1 from Bcl-2, which, in turn, induces autophagy [26, 30, 31]. Basal interaction between Beclin1 and the Bcl-2/Bcl-xL is prerequisite for these mechanisms to be able to activate autophagy. However, the binding affinity of Bcl-2/Bcl-xL to Beclin1 is low except in the case of Bcl-2 encoded by Kaposi's sarcoma-associated herpesvirus[11, 23, 24]. Then how can the basal interaction between Beclin1 and Bcl-2/Bcl-xL take place? We here demonstrate that Mst1-induced phosphorylation of Beclin1 in its BH3 domain at Thr^{108} promotes

binding of Beclin1 with Bcl-2/Bcl-xL. Since interaction between Beclin1 and Bcl-2/Bcl-xL is markedly reduced when Mst1 activity is inhibited, Mst1 is likely to be a physiological kinase mediating the basal interaction between Beclin1 and Bcl-2/Bcl-xL.

The Beclin1 CCD acts as a central interaction platform for either homodimerization in its inactive form or heterodimerization with Atg14L to stimulate autophagy. Crystallographic analyses showed that the CCDs of two Beclin1 molecules can associate with each other in an antiparallel orientation, forming a metastable structure that readily transits into a stable heterodimer complex with the CCD of Atg14L [22]. A previous study and our experiments demonstrate that not only does the Beclin1 BH3 domain interact with the Bcl-2/Bcl-xL hydrophobic groove, but the Beclin1 CCD interacts with the Bcl-2/Bcl-xL BH4 domain as well [32]. Thus, Beclin1 interacts with Bcl-2 at two sites, and the interaction at one of them is regulated by Mst1. This should allow Bcl-2 to bridge two Beclin1 molecules in an Mst1-sensitive manner, with the Beclin1 dimer further stabilized by alignment of the CCDs in an anti-parallel orientation [22, 32]. Since Beclin1-Atg14L interaction is significantly enhanced by inhibition of endogenous Mst1 *in vivo*, Mst1-induced phosphorylation of Beclin1 and consequent stabilization of the Beclin1 homodimer may cause dissociation of Atg14L from Beclin1, thereby diminishing the activity of Vps34 in the Ag14L-Vps34 complex.

In this study, we found that Mst1 facilitates the molecular link between Beclin1 and Bcl-2, thereby not only negatively regulating autophagy, but also positively regulating apoptosis by promoting sequestration of the Bcl-2 family proteins from Bax. Suppression of autophagy exacerbates protein aggregation while stimulation of apoptosis directly leads to decreased cardiac contractility in the failing heart. Thus, inhibition of Mst1 may effectively alleviate these problems in heart failure patients. The *Hippo* pathway has recently emerged as a tumor suppressor signaling pathway [33]. Dual regulation of autophagy and apoptosis may enhance the function of Mst1 as a tumor suppressor by eliminating an adaptive mechanism for survival in a hypoxic environment and promoting cell death.

In summary, enhancement of Beclin1-Bcl-2 interaction through phosphorylation of Beclin1 in its BH3 domain at Thr^{108} by Mst1 inhibits autophagy and induces apoptosis, which, when autophagic activity falls below the required level, impairs protein quality control and induces cardiac dysfunction (Supplementary Fig. 7).

Online Methods

Genetically modified mice

Heterozygous GFP-LC3 transgenic (Tg-GFP-LC3) mice (C57BL/6J background, strain GFP-LC3#53, RIKEN BioResource Center) containing a rat LC3-EGFP fusion under control of the chicken β-actin promoter, homozygous Mst1 knock-out ($Mst1^{-/-}$) mice (C57BL/6J background), heterozygous Beclin1 knock-out ($Beclin1^{+/-}$) mice (C57BL/6J background), and transgenic mice with cardiac-specific overexpression of Mst1 (Tg-Mst1) and DN-Mst1 (Tg-DN-Mst1, C57BL/6J background) [14] were bred in-house. We used age-matched male mice in all animal experiments. All animal protocols were approved by the Institutional Animal Care and Use Committee of the University of Medicine and Dentistry of New Jersey.

Human samples from explanted hearts

The samples from explanted hearts used in this study were obtained from 6 patients who had received heart transplants and 6 age-matched donors (listed in the Supplementary Table) at the Taipei Veterans General Hospital. The study was approved by the institutional Ethics Committee (VGHIRB No.:2012-06-028D), and all patients or their family expressed their willingness to participate through an informed consent form. Myocardial posterior wall samples were collected during preparation of donor hearts for transplantation in the hospital. Myocardial samples from near the mitral annulus were obtained from recipients at the time of therapeutic transplantation. Immediately after tissue procurement, the samples for biochemical study were stored in liquid nitrogen and kept at −80°C. Selected samples for immunohistochemical analysis were fixed in 4% paraformaldehyde in phosphate-buffered saline (pH 7.4), paraffin-embedded and sectioned.

Primary culture of neonatal rat ventricular CMs

Primary cultures of ventricular CMs were prepared from 1-day-old Crl: (WI) BR-Wistar rats (Harlan Laboratories, Somerville, NJ, USA) as described previously [34]. A CM-rich fraction was obtained by centrifugation through a discontinuous Percoll gradient.

Mouse embryonic fibroblasts (MEFs)

$Bax^{-/-}Bak^{-/-}$ MEFs were kindly provided by Richard N. Kitsis (Albert Einstein University, Bronx, NY). MEFs deficient in Mst1 were harvested from $Mst1^{-/-}$ mice. To make $Mst1^{-/-}Mst2^{-/-}$ MEFs, MEFs were harvested from $Mst1^{-/-}Mst2^{flox/flox}$ mice and then stably transfected with MCMV-neo-Cre. $Atg7^{-/-}$ MEFs were harvested from $Atg7^{flox/flox}$ mice provided by Dr. Masaaki Komatsu (Tokyo Metropolitan Institute of Medical Science, Tokyo, Japan) and stably transfected with MCMV-neo-Cre. MEF cells were cultured at 37°C and 5% CO_2 in DMEM supplemented with 10% fetal bovine serum.

Antibodies and reagents

The following commercial antibodies were used: phospho-Mst1 [Thr^{183}](#ab79199, 1:1,000 for WB), TGN46 (2F7.1, #ab2809, 1:100 for IHC) and Vimentin (#ab71144, 1:100 for IHC) (abcam); Mst1 (7/MST1, #611052, 1:1,000 for WB), Bcl-2 (#554087, 1:1,000 for WB) and Bcl-xL (#610747, 1:1,000 for WB)(BD Bioscience); Cleaved caspase-3 (D3E9, #9579, 1:1,000 for WB), Cytochrome *c* (#4272, 1:1,000 for WB), DYKDDDDK (Flag)-tag (#2368, 1:2,000 for WB), HA-tag (C29F4, #3724, 1:2,000 for WB), Histone H3 (#9717, 1:1,000 for WB), Myc-tag (conjugated to magnetic beads)(9B11, #5698), Sav1 (WW45)(#3507, 1:1,000 for WB), ULK1 (D8H5, #8054, 1:1,000 for WB), UVRAG (#5320, 1:1,000 for WB), Vps34 (D9A5, #4263, 1:1,000 for WB) and secondary antibodies (Anti-mouse/rabbit IgG) conjugated with horseradish peroxidase (Cell Signaling); Secondary antibodies (Anti-mouse/rabbit IgG) conjugated with Alexa Fluor® 488, Alexa Fluor® 555 or Alexa Fluor® 647 (Life Technologies); Bax (6A7, #AM44, 1:1,000 for WB)(Merck-Millipore); Atg4B (9H5, #M134-3, 1:1,000 for WB), Atg5 (#PM050, 1:1,000 for WB), Atg7 (#PM039, 1:1,000 for WB), LC3 (8E10, #M186-3, 1:1,000 for WB), Atg14L (#PD026, 1:1,000 for WB) and Rubicon (#PD027, 1:1,000 for WB)(MBL); p62/SQSTM1 (TA307334, 1:1,000 for WB; 1:100 for IHC) and Mst2 (STK3, EP1466Y, #TA300843, 1:1,000 for WB)(Origene

Technologies); Troponin T (Ab-1, #MS-295-P, 1:500 for IHC)(Thermo Scientific); α-actinin (H-300, #sc-15335, 1:2,000 for WB), Bax (P-19, #sc-526, 1:1,000 for WB), Bak (G-23, #sc-832, 1:1,000 for WB), Beclin1 (H-300, #sc-11427, 1:1,000 for WB), Troponin I (H-170, #sc-15368, 1:200 for IHC) and poly-ubiquitin (P4D1, #sc-8017, 1:1,000 for WB; 1:100 for IHC)(Santa Cruz); GAPDH (#G9545, 1:2,000 for WB), tubulin (DM1A, #T9026; 1:2,000 for WB), HA-tag (conjugated to agarose beads)(HA-7, #A2095), Flag-tag (conjugated to agarose beads)(FLAG-M2, #A2220), ULK1 (#A7481, 1:1,000 for WB) and mouse control IgG (Sigma Aldrich); and KDEL (10C3, #ADI-SPA-827, 1:2,000 for WB; 1:100 for IHC) and CryAB (ADI-SPA-224, 1:100 for IHC)(ENZO). For detection of phosphorylation of Beclin1 at Thr^{108}, a rabbit polyclonal phosphorylation-specific antibody was raised against a synthetic peptide of the BH3 domain of human Beclin1, EASDGG{T-p}MENLSRR (1:500 for WB; 1:50 for IHC). Mouse monoclonal antibody against Lats2 has been described (1:1,000 for WB; 1:100 for IHC) [35]. Alexa Fluor® 555 phalloidin and Alexa Fluor® 647 MitoTracker® Deep Red FM were purchased from Life Technologies. Chloroquine diphosphate was purchased from Fluka Biochemika. ABT-737 was purchased from Selleck Chemicals.

Immunoblotting

Cardiomyocytes were lysed with RIPA buffer. Lysates were centrifuged at 13,200 rpm for 15 min at 4°C. Electrophoresis was performed on Laemmli-SDS-polyacrylamide gels. Separated proteins were transferred from the gels to PVDF membranes by semi-dry electrotransfer and immunoblotting was performed as previously described [36].

Native PAGE

Recombinant Beclin1 was dissolved in a buffer containing 50 mM Tris-HCl buffer (pH 7.4), 1 mM EDTA and 150 mM NaCl at a concentration of 1 μg/mL at 4 °C. Beclin1 protein was incubated with Bcl-2 protein after kinase reaction with or without Mst1 and the proteins were crosslinked by UV in the presence of sulfo-NHS-SS-diazirine. The protein samples were mixed with an electrophoretic sample buffer (40% v/v glycerol containing 0.01% bromophenol blue) and separated on a 7.5% polyacrylamide gel in a 90 mM Tris-borate buffer system and 1 mM EDTA (pH 8.0) at 200 V for 2 h. The protein bands were visualized using 0.25% (w/v) Coomassie Brilliant Blue R-250.

Fractionation

Endoplasmic reticulum fractionation was performed with the ER enrichment kit from IMGENEX. After suspension in 1.5 mL of 1x isosmotic homogenization buffer, the cultured cardiomyocytes were homogenized and centrifuged for 10 min at 1,000 x g at 4°C. The supernatant was transferred into a new tube and centrifuged for 15 min at 12,000 x g at 4°C to eliminate the mitochondria and the cell debris. The resulting supernatant was ultracentrifuged at 90,000 x g for 1 h at 4°C. The pellet containing the ER was resuspended in 1x suspension buffer containing protease inhibitors. Mitochondrial and cytosolic fractions were collected as described previously [37]. Briefly, cultured cardiomyocytes were resuspended in hypotonic lysis buffer (10 mM K-HEPES (pH 7.9), 1.5 mM $MgCl_2$, 10 mM KCl, 0.2 mM Na_3VO_4, 1 mM DTT, 1% Protease Inhibitor Cocktail) and homogenized. Whole cell lysates were centrifuged at 60 x g for 5 min. The supernatant was collected, and

the homogenization and centrifugation was repeated on the pellet. The total homogenate was centrifuged at 1,200 x g to separate the pellet from cell membrane and cytosolic proteins. The supernatant of the total homogenate was centrifuged at 3,500 x g for 20 min to separate mitochondrial fractions. To separate cytosolic fractions, the supernatant was further centrifuged at 100,000 x g for 60 min.

Immunoprecipitation

CMs were lysed with IGEPAL CA-630 buffer (50 mM Tris-HCl (pH 7.4), 1% IGEPAL CA-630, 10 mM EDTA, 150 mM NaCl, 50 mM NaF, 1 μM leupeptin and 0.1 μM aprotinin). Primary antibody was covalently immobilized on protein A/G agarose using the Pierce® Crosslink Immunoprecipitation Kit according to the manufacturer's instructions (Thermo Scientific). Samples were incubated with immobilized antibody beads for at least 2 h at 4°C. After IP, the samples were washed with TBS five times. They were then eluted with glycine-HCl (0.1 M, pH 3.5) and the immunoprecipitates were subjected to immunoblotting using specific primary antibodies and conformation-specific secondary antibody that recognizes only the native IgG (Cell Signaling).

Recombinant proteins

In order to generate GST-Mst1, GST-Beclin1, GST-Bcl-2, and GST-Bcl-xL (full-length and fragment, wild-type and mutant), we used the pCold-GST vector (courtesy of C. Kojima, Nara Institute of Science and Technology, Ikoma, Nara, Japan) [38]. Proteins fused to glutathione S-transferase (GST) were expressed in *E. coli* strain BL21 (DE3) cultured in LB medium containing 100 μg/mL ampicillin. Protein expression was induced by addition of 1 mM IPTG after lowering the temperature from 37°C to 15°C. Cells were cultured for 16 h following induction and purified with glutathione Sepharose 4B (GE Healthscience). In order to remove the N-terminal GST tag, the recombinant protein immobilized on glutathione Sepharose 4B was digested at 4°C with GST-tagged human rhinovirus (HRV) 3C protease (PreScission protease, GE Healthcare).

Pull-down binding assays

A GST-tagged fusion protein was digested to remove the GST tag, then mixed with 500 μL of PBS containing 0.5% Triton X-100 and incubated for 30 min at 4°C. A slurry of glutathione Sepharose 4B in which a second GST-tagged fusion protein was immobilized was added, followed by further incubation for 30 min at 4°C. After washing three times with phosphate-buffered saline, proteins were eluted with 2x SDS sample buffer. The eluates were subjected to SDS-PAGE and proteins were detected by immunoblot.

In vitro kinase assays

In vitro kinase assays were carried out as described with modifications [36]. Recombinant active Mst1 (10 ng) (Millipore) was incubated with full-length or fragmented Beclin1 (1 μg) in a kinase buffer (50 mM HEPES (pH 7.4), 15 mM $MgCl_2$ and 200 μM sodium vanadate containing 100 μM ATP or 5 μM ATP and 10 μCi [γ-^{32}P] ATP per reaction) at 30°C for 30 min. Phosphorylated proteins were separated by SDS-PAGE and analyzed by autoradiography.

Construction of adenoviruses

Recombinant adenovirus vectors were constructed, propagated and titered as previously described [34]. Briefly, pBHGloxΔE1,3 Cre (Microbix), including the ΔE1 adenoviral genome, was co-transfected with the pDC316 shuttle vector containing the gene of interest into HEK293 cells using LipofectAMINE 2000 (Life Technologies). Through homologous recombination, the test genes were integrated into the E1-deleted adenoviral genome. The viruses were propagated in HEK293 cells. We made replication-defective human adenovirus type 5 (devoid of E1) harboring 3xFlag-Mst1-WT, 3xFlag-Beclin1-WT, Beclin1-T108A mutant, Beclin1-T108D mutant, 3xFlag-Vps34-WT, Atg14-WT-2xHA, myc-Bcl-2-WT and GFP-2xFYVE. The mutant Beclin1 plasmids were generated by site-directed mutagenesis. All mutations were verified by sequencing. The generation of adenoviruses harboring Mst1-WT, DN-Mst1 [K59R], Beclin1-WT, JNK1, GFP-LC3 and mRFP-GFP-LC3 has been described [4, 14, 19]. Adenovirus harboring β-galactosidase (Ad-LacZ) was used as a control.

Construction of short hairpin RNA (shRNA) adenoviral expression vectors

The pSilencer 1.0-U6 expression vector was purchased from Ambion. The U6 RNA polymerase III promoter and the polylinker region were subcloned into the adenoviral shuttle vector pDC311 (Microbix). The Mst1 shRNA targeting sequence was: 5'-AGACCGTGCAACTGAGGAAC-3'. The Bcl-2 shRNA targeting sequence was: 5'-GGGAGAACAGGGTATGATA-3'. The Bcl-xL shRNA targeting sequence was: 5'-GGAGATGCAGGTATTGGTG-3'. The Bax shRNA targeting sequence was: 5'-CTCCGGCGAATTGGAGATGAA-3'. Recombinant adenoviruses were generated by homologous recombination in HEK293 cells as described above.

Lipid kinase assay

Ad-3xFlag-Vps34, Ad-Beclin1-WT, Ad-Beclin1-T108A or Ad-Beclin1-T108D, and Ad-Mst1 or Ad-LacZ were co-transduced into CMs. Cells were lysed in lysis buffer (1% IGEPAL CA-630, 20 mM Tris-HCl (pH 7.5), 137 mM NaCl, 1 mM $MgC1_2$, 1 mM $CaC1_2$, 100 mM NaF, 10 mM sodium pyrophosphate, 100 μM Na_3VO_4, 10% glycerol, 0.35 mg/mL PMSF, and protease and phosphatase inhibitor cocktails). After immunoprecipitation, beads (associated with complexed proteins) were washed three times in lysis buffer, followed by three washes in a washing buffer (100 mM Tris-HCl (pH 7.4) and 500 mM LiCl) and two washes in a reaction buffer (10 mM Tris-HCl (pH 7.4), 100 mM NaCl and 1 mM EDTA). Beads were resuspended in 60 μL of reaction buffer and 10 μL of 100 mM $MnCl_2$ and sonicated, followed by the addition of 10 μL of 2 μg/μL phosphatidylinositol. The reaction was started by the addition of ATP (10 μL of 440 μM ATP containing [γ-^{32}P] ATP (10 μCi)), and beads were incubated for 10 min at room temperature. The reaction was terminated by adding 20 μL of 8 M HCl, and the organic phase was extracted with 160 μL chloroform:methanol (1:1). Extracted phospholipid products were resolved by thin-layer chromatography (TLC) using a coated silica gel and a solvent composed of chloroform: methanol: H_2O: NH_4OH (v/v/v/v, 9:7:1.7:0.3). Phosphorylated radioactive phosphatidylinositol 3-phosphate (PtdIns(3,4,5)P_3), a reaction product separated by TLC, was visualized by autoradiography. The radioactive PtdIns(3,4,5)P_3 was then excised from the thin layer plates and assayed in a liquid scintillation β-counter (LSC).

Long-lived protein degradation assay

Neonatal rat CMs plated in 12-well plates were transduced with Ad-LacZ, Ad-Mst1, Ad-DN-Mst1 or Ad-sh-Mst1. After 48 h, intracellular proteins were labeled for 18 h at 37°C with ^{3}H-l-valine (1 μCi/mL) in DMEM. After being pulse-labeled for 24 h, cells were washed three times and cultured in DMEM supplemented with excess unlabeled valine (10 mM) for 16 h to chase out short-lived proteins. Cells were then washed and further cultured for 4 h in complete medium or Earle balanced salt solution (EBSS) containing unlabeled valine (10 mM). Both media and cell lysates were subjected to trichloroacetic acid (TCA) precipitation. Long-lived protein degradation was calculated as the ratio of TCA-soluble medium to TCA-precipitated cell lysate radioactivity.

Mass spectrometry

Two peptides containing partial human Beclin1 amino acid sequences were prepared as follows: NT1 peptide (88–100 AA of Beclin1: MMSTESANSFTLI) and NT2 peptide (102–121 AA of Beclin1: EASDGGTMENLSRRLKVTGD). After a kinase reaction with Mst1, the samples were analyzed on a 4700 Proteomics Analyzer tandem mass spectrometer (Life Technologies). Positive ion mass spectra were acquired in the reflectron mode. Tandem mass spectra of selected ions were acquired using a method optimized with 1 kV collision energy. Data analysis was performed with Data Explorer software (Life Technologies).

Immunohistochemistry

Neonatal CMs were cultured on coverslips, transduced with adenoviruses and fixed in 4% paraformaldehyde. Mouse hearts were fixed with 4% paraformaldehyde by perfusion and sectioned at 10 μm thickness. De-paraffinized tissue sections were antigen unmasked using citrate buffer. Samples were permeabilized with PBST (0.3% Triton X-100 in PBS), and nonspecific binding was blocked with 5% goat serum in PBST for 90 min. For immunofluorescent staining, an overnight incubation with specific antibodies was followed by 2 h of incubation with Alexa Fluor® 488, 555, 594 or 647 Dye-conjugated secondary antibody (Life Technologies). Samples were washed and mounted on glass slides with a reagent containing 4′, 6-diamino-2-phenilindole (DAPI) (VECTASHIELD; Vector Laboratories). Cells were observed under a fluorescence microscope (Eclipse E800, Nikon) or with a laser-scanning confocal image system (A1, Nikon).

Fluorescence microscopic detection of GFP-LC3 or mRFP-GFP-LC3

CMs grown on gelatinized coverslips were transduced with Ad-GFP-LC3 or Ad-mRFP-GFP-LC3. After 48 h, media were changed to complete, glucose-free or amino acid-free medium, with or without chloroquine. Tissue samples for GFP observation were fixed with 4% paraformaldehyde in PBS. The fixed tissues were treated with 15% sucrose in PBS for 4 h and then with 30% sucrose solution overnight. Tissue samples were embedded in Tissue-Tek OCT compound (Sakura Finetechnical Co.Ltd) and stored at −70°C. The samples were sectioned at 5–7 μm thickness with a cryostat (CM3050 S, Leica), air-dried for 30 min, and stored at −20°C. The fluorescence of GFP-LC3 or mRFP-GFP-LC3 was observed under a fluorescence microscope as previously described [19, 39]. The number of GFP-LC3 or mRFP-GFP-LC3 puncta was counted in five independent visual fields.

Detection of aggresomes

The ProteoStat® Aggresome Detection Kit and anti-fade mounting medium were purchased from Enzo Life Sciences. The ProteoStat® aggresome detection reagent is a 488 nm excitable red fluorescent molecular rotor that binds selectively to protein cargo within aggresomes in cells. All components of the ProteoStat® Aggresome Detection Kit were prepared according to the manufacturer's instructions [40]. One mM stock solutions of the dyes were prepared in DMSO.

Phosphatidylinositol 3-kinase (PI3K) assay *in situ*

To measure the abundance of membrane-associated phosphatidyl inositol-3-phosphate in order to evaluate the activity of the Beclin1/Vps34 complex *in situ*, we generated Ad-GFP-2xFYVE, which harbors the FYVE (**F**ab1, **Y**OTB, **V**ac1p and **E**EA1) domain. The amino acid sequence we used for this adenovirus construction was as follows: NH_2-WVPDSQAPNCMKCEARFTFTK**RRHHCRACG**KVFCASCCSLKCKLLYMDRKEARV CVICHSVL-COOH. This assay was performed as detailed previously [41, 42]. CMs grown on gelatinized coverslips were transduced with Ad-Mst1, Ad-DN-Mst1, Ad-sh-Mst1, Ad-LacZ, Ad-Beclin1-WT, Ad-Beclin1-T108A or Ad-Beclin1-T108D 24 h after Ad-GFP-2xFYVE transduction. After 48 h, media were changed to complete or glucose-free medium, and cells were treated with or without 3-MA (5 mM) for 2 h. Cells were fixed with 4% paraformaldehyde in PBS for 15 min. The number of GFP-2xFYVE dots in cytoplasm was counted in five independent visual fields.

Electron microscopy

Heart tissue was removed from the animal and quickly rinsed in PBS. The tissue was placed in a petri dish with 0.5% gluteraldehyde and 0.2% tannic acid in PBS and diced into 2 mm cubes, then transferred to modified Karnovsky's fixative (4% formaldehyde and 2.5% gluteraldehyde containing 8 mM $CaCl_2$ in 0.1 M sodium cacodylate buffer (pH 7.4)). Samples were washed with PBS and post-fixed in 1% osmium tetroxide in 0.1 M sodium cacodylate buffer (pH 7.4) for 1 h to produce osmium black. Samples were then dehydrated through a graded series of ethanol and embedded in Epon/SPURR resin (EM Science) that was polymerized at 65°C overnight. Sections of both heart tissues and yeast cells were prepared with a diamond knife on a Reichert-Jung Ultracut-E ultra-microtome and stained with UrAc (20 min) followed by 0.2% lead citrate (2.5 min). Images were photographed with a Jeol JEM-1200EX electron microscope.

MI Surgery

Transgenic and nontransgenic male mice, 3 to 4 months old, were used in this study. The mice were anesthetized by intraperitoneal injection of pentobarbital sodium (60 mg/kg), and were ventilated via tracheal intubations connected to a rodent ventilator during the surgical procedure. A left thoracotomy was performed through the third intercostal space, and the left anterior descending branch of the coronary artery was visualized. Under direct microscopic control, an 8-0 nylon suture was placed around the vessel and ligated ~1.0 to 2.0 mm from the tip of the normally positioned left auricle. The chest wall was then closed in layers using 5-0 nylon sutures. Additional age-matched sham-operated control animals underwent a

similar surgery without ligation of the artery. The mice were extubated and allowed to recover in a cage with the temperature maintained at 37°C overnight.

Echocardiography

Echocardiography was performed as described previously [14] with a 13-MHz linear ultrasound transducer. Two-dimensional guided M-mode measurements of LV internal diameter were obtained from at least three beats and then averaged. LV end-diastolic dimension (LVEDD) was measured at the time of the apparent maximal LV diastolic dimension, and LV end-systolic dimension (LVESD) was measured at the time of the most anterior systolic excursion of the posterior wall. LVEF was calculated using the following formula: LVEF (%)=100 x ($LVEDD^3$ - $LVESD^3$) / $LVEDD^3$.

Assessment of LV scar size after chronic MI

Hearts were fixed in 10% formalin, cut into 4 transverse slices and subjected to Masson's Trichrome staining for measurement of the LV scar after chronic MI. The average infarct size was obtained by calculation of the average length of the circumference in the infarct portion and the normal area from consecutive myocardial slices as shown in Supplementary Figure 1c.

TUNEL staining in cultured cardiomyocytes

Cardiomyocytes were fixed in PBS containing 4% paraformaldehyde. Staining was performed using the In Situ Cell Death Detection kit (Roche) as described [43].

Viability of the cells

Viability of the cells was measured by Cell Titer Blue assays (Promega) as previously described [43].

Statistics

Statistical analyses between groups were done by unpaired Student's *t* test or one-way ANOVA followed by a post hoc Fisher's comparison test. A value of less than 0.05 was considered significant. Survival curves were analyzed by Kaplan-Meier-Log-rank (Mentel-Cox) test. Statistical analyses were done using GraphPad Prism (GraphPad Software, Inc.).

Supplementary Material

Refer to Web version on PubMed Central for supplementary material.

ACKNOWLEDGEMENTS

We thank C. Brady for critical reading of the manuscript and Y. Ikeda, Y. Matsuda and N. Tamura for their excellent technical assistance. We also thank N. Mizushima, T. Yoshimori, M. Komatsu, R. Kitsis and B. Levine for mice, cells and reagents. This work was supported in part by US Public Health Service Grants HL59139, HL67724, HL69020, HL91469, HL102738, AG27211, the Foundation of Leducq Transatlantic Network of Excellence (J.S.), American Heart Association Scientist Development Grant 12SDG12070262, and the Banyu Fellowship Program sponsored by Banyu Life Science Foundation International (Y.M.).

References

1. Levine B, Klionsky DJ. Development by self-digestion: molecular mechanisms and biological functions of autophagy. Dev Cell. 2004; 6:463–477. [PubMed: 15068787]
2. Nakai A, et al. The role of autophagy in cardiomyocytes in the basal state and in response to hemodynamic stress. Nat Med. 2007; 13:619–624. [PubMed: 17450150]
3. Yan L, et al. Autophagy in chronically ischemic myocardium. Proc Natl Acad Sci U S A. 2005; 102:13807–13812. [PubMed: 16174725]
4. Matsui Y, et al. Distinct roles of autophagy in the heart during ischemia and reperfusion: roles of AMP-activated protein kinase and Beclin 1 in mediating autophagy. Circ Res. 2007; 100:914–922. [PubMed: 17332429]
5. Zhu H, et al. Cardiac autophagy is a maladaptive response to hemodynamic stress. J Clin Invest. 2007; 117:1782–1793. [PubMed: 17607355]
6. Shih H, Lee B, Lee RJ, Boyle AJ. The aging heart and post-infarction left ventricular remodeling. J Am Coll Cardiol. 2011; 57:9–17. [PubMed: 21185495]
7. Pattingre S, et al. Bcl-2 antiapoptotic proteins inhibit Beclin 1-dependent autophagy. Cell. 2005; 122:927–939. [PubMed: 16179260]
8. Mizushima N, Komatsu M. Autophagy: renovation of cells and tissues. Cell. 2011; 147:728–741. [PubMed: 22078875]
9. Liang XH, et al. Protection against fatal Sindbis virus encephalitis by beclin, a novel Bcl-2-interacting protein. J Virol. 1998; 72:8586–8596. [PubMed: 9765397]
10. Kihara A, Noda T, Ishihara N, Ohsumi Y. Two distinct Vps34 phosphatidylinositol 3-kinase complexes function in autophagy and carboxypeptidase Y sorting in Saccharomyces cerevisiae. J Cell Biol. 2001; 152:519–530. [PubMed: 11157979]
11. Itakura E, Kishi C, Inoue K, Mizushima N. Beclin 1 forms two distinct phosphatidylinositol 3-kinase complexes with mammalian Atg14 and UVRAG. Mol Biol Cell. 2008; 19:5360–5372. [PubMed: 18843052]
12. Funderburk SF, Wang QJ, Yue Z. The Beclin 1–VPS34 complex – at the crossroads of autophagy and beyond. Trends in Cell Biology. 2010; 20:355–362. [PubMed: 20356743]
13. Pan D. The hippo signaling pathway in development and cancer. Dev Cell. 2010; 19:491–505. [PubMed: 20951342]
14. Yamamoto S, et al. Activation of Mst1 causes dilated cardiomyopathy by stimulating apoptosis without compensatory ventricular myocyte hypertrophy. J Clin Invest. 2003; 111:1463–1474. [PubMed: 12750396]
15. Del Re DP, et al. Proapoptotic Rassf1A/Mst1 signaling in cardiac fibroblasts is protective against pressure overload in mice. J Clin Invest. 2010; 120:3555–3567. [PubMed: 20890045]
16. Odashima M, et al. Inhibition of endogenous Mst1 prevents apoptosis and cardiac dysfunction without affecting cardiac hypertrophy after myocardial infarction. Circ Res. 2007; 100:1344–1352. [PubMed: 17395874]
17. Gautreau A, et al. Isolation and characterization of an aggresome determinant in the NF2 tumor suppressor. J Biol Chem. 2003; 278:6235–6242. [PubMed: 12471027]
18. Rote KV, Rechsteiner M. Degradation of microinjected proteins: effects of lysosomotropic agents and inhibitors of autophagy. J Cell Physiol. 1983; 116:103–110. [PubMed: 6853609]
19. Hariharan N, et al. Deacetylation of FoxO by Sirt1 Plays an Essential Role in Mediating Starvation-Induced Autophagy in Cardiac Myocytes. Circ Res. 2010; 107:1470–1482. [PubMed: 20947830]
20. Roggo L, et al. Membrane transport in Caenorhabditis elegans: an essential role for VPS34 at the nuclear membrane. EMBO J. 2002; 21:1673–1683. [PubMed: 11927551]
21. Maiuri MC, et al. Functional and physical interaction between Bcl-X(L) and a BH3-like domain in Beclin-1. EMBO J. 2007; 26:2527–2539. [PubMed: 17446862]
22. Li X, et al. Imperfect interface of Beclin1 coiled-coil domain regulates homodimer and heterodimer formation with Atg14L and UVRAG. Nat Commun. 2012; 3:662. [PubMed: 22314358]

23. Zhong Y, et al. Distinct regulation of autophagic activity by Atg14L and Rubicon associated with Beclin 1-phosphatidylinositol-3-kinase complex. Nature Cell Biology. 2009; 11:468–476. [PubMed: 19270693]
24. Matsunaga K, et al. Two Beclin 1-binding proteins, Atg14L and Rubicon, reciprocally regulate autophagy at different stages. Nature Cell Biology. 2009; 11:385–396. [PubMed: 19270696]
25. Sun Q, et al. Identification of Barkor as a mammalian autophagy-specific factor for Beclin 1 and class III phosphatidylinositol 3-kinase. Proc Natl Acad Sci U S A. 2008; 105:19211–19216. [PubMed: 19050071]
26. Zalckvar E, et al. DAP-kinase-mediated phosphorylation on the BH3 domain of beclin 1 promotes dissociation of beclin 1 from Bcl-XL and induction of autophagy. EMBO Rep. 2009; 10:285–292. [PubMed: 19180116]
27. Oberstein A, Jeffrey PD, Shi Y. Crystal structure of the Bcl-XL-Beclin 1 peptide complex: Beclin 1 is a novel BH3-only protein. J Biol Chem. 2007; 282:13123–13132. [PubMed: 17337444]
28. Ross CA. pinion: What is the role of protein aggregation in neurodegeneration? Nat Rev Mol Cell Biol. 2005; 6:891–898. [PubMed: 16167052]
29. Tannous P, et al. Intracellular Protein Aggregation Is a Proximal Trigger of Cardiomyocyte Autophagy. Circulation. 2008; 117:3070–3078. [PubMed: 18541737]
30. Wei Y, Pattingre S, Sinha S, Bassik M, Levine B. JNK1-mediated phosphorylation of Bcl-2 regulates starvation-induced autophagy. Mol Cell. 2008; 30:678–688. [PubMed: 18570871]
31. He C, et al. Exercise-induced BCL2-regulated autophagy is required for muscle glucose homeostasis. Nature. 2012; 481:511–515. [PubMed: 22258505]
32. Noble CG, Dong JM, Manser E, Song H. Bcl-xL and UVRAG cause a monomer-dimer switch in Beclin1. J Biol Chem. 2008; 283:26274–26282. [PubMed: 18641390]
33. Harvey K, Tapon N. The Salvador-Warts-Hippo pathway - an emerging tumour-suppressor network. Nat Rev Cancer. 2007; 7:182–191. [PubMed: 17318211]
34. Ago T, et al. A redox-dependent pathway for regulating class II HDACs and cardiac hypertrophy. Cell. 2008; 133:978–993. [PubMed: 18555775]
35. Yabuta N, et al. Structure, expression, and chromosome mapping of LATS2, a mammalian homologue of the Drosophila tumor suppressor gene lats/warts. Genomics. 2000; 63:263–270. [PubMed: 10673337]
36. Maejima Y, et al. Nitric oxide inhibits ischemia/reperfusion-induced myocardial apoptosis by modulating cyclin A-associated kinase activity. Cardiovasc Res. 2003; 59:308–320. [PubMed: 12909314]
37. Matsushima S, et al. Increased oxidative stress in the nucleus caused by Nox4 mediates oxidation of HDAC4 and cardiac hypertrophy. Circ Res. 2013; 112:651–663. Epub 272012 Dec 279727. [PubMed: 23271793]
38. Hayashi K, Kojima C. pCold-GST vector: a novel cold-shock vector containing GST tag for soluble protein production. Protein Expr Purif. 2008; 62:120–127. [PubMed: 18694833]
39. Mizushima N, Yamamoto A, Matsui M, Yoshimori T, Ohsumi Y. In vivo analysis of autophagy in response to nutrient starvation using transgenic mice expressing a fluorescent autophagosome marker. Mol Biol Cell. 2004; 15:1101–1111. [PubMed: 14699058]
40. Shen D, et al. Novel cell- and tissue-based assays for detecting misfolded and aggregated protein accumulation within aggresomes and inclusion bodies. Cell Biochem Biophys. 2011; 60:173–185. [PubMed: 21132543]
41. Gillooly DJ, et al. Localization of phosphatidylinositol 3-phosphate in yeast and mammalian cells. EMBO J. 2000; 19:4577–4588. [PubMed: 10970851]
42. Shi CS, Kehrl JH. TRAF6 and A20 regulate lysine 63-linked ubiquitination of Beclin-1 to control TLR4-induced autophagy. Sci Signal. 2010; 3:ra42. [PubMed: 20501938]
43. Sciarretta S, et al. Rheb is a critical regulator of autophagy during myocardial ischemia: pathophysiological implications in obesity and metabolic syndrome. Circulation. 125:1134–1146. [PubMed: 22294621]

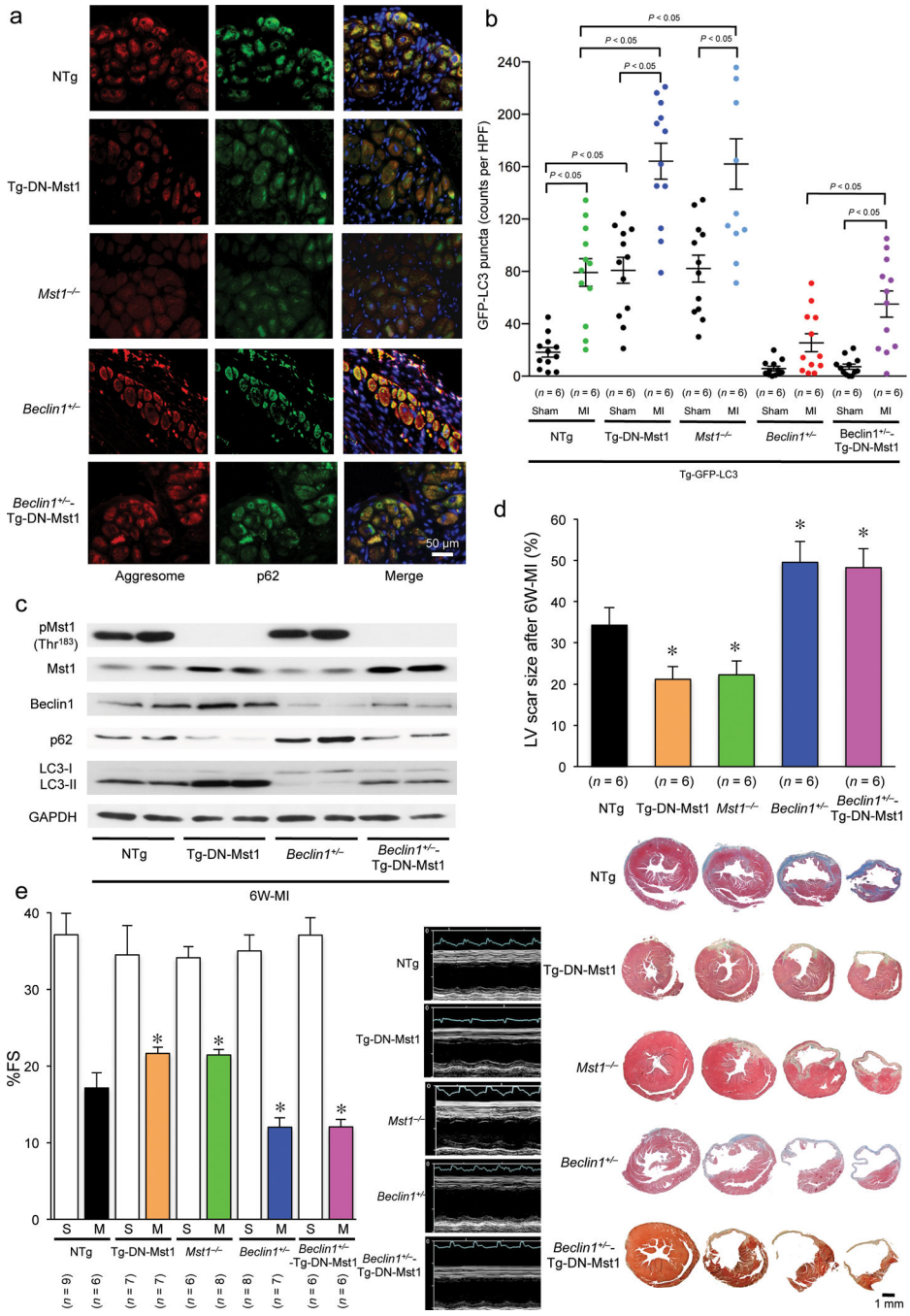

Figure 1. Suppression of autophagy during chronic phase of MI is detrimental for cardiac remodeling

(**a**) Representative immunofluorescent images of staining with p62/SQSTM1 (green), DAPI (blue), and ProteoStat® aggresome detection reagent (red) in Tg-DN-Mst1, *Mst1*$^{-/-}$ *Beclin1*$^{+/-}$ *Beclin1*$^{+/-}$-Tg-DN-Mst1, and NTg mice 6 weeks after coronary artery ligation are shown. Results represent means from 4 independent experiments. (**b**) Quantitative analysis of the number of GFP-LC3 puncta 6 weeks after coronary artery ligation in Tg-DN-Mst1, *Mst1*$^{-/-}$ *Beclin1* $^{+/-}$ *Beclin1*$^{+/-}$-Tg-DN-Mst1, and NTg mice that were crossed with Tg-GFP-

LC3 mice is shown. Representative images of GFP-LC3 puncta are shown in Supplementary Figure 1a. Data are reported as mean ± SEM. (**c**) Representative immunoblot images of heart homogenates from Tg-DN-Mst1, *Mst1*$^{-/-}$ *Beclin1*$^{+/-}$ *Beclin1*$^{+/-}$ -Tg-DN-Mst1, and NTg mice with phospho-Mst1 (Thr^{183}), total Mst1, total Beclin1, p62/SQSTM1, LC3, and GAPDH antibodies after 6 weeks of MI are shown. Results represent means from 3 independent experiments. (**d**) *Upper:* Quantitative analysis of the LV scar size in Tg-DN-Mst1, *Mst1*$^{-/-}$ *Beclin1*$^{+/-}$ *Beclin1*$^{+/-}$ -Tg-DN-Mst1, and NTg mice after 6 weeks of MI is shown. Data are reported as mean ± SEM. * $P < 0.05$ vs NTg mice after 6-week MI. *Lower:* Representative images of four consecutive myocardial slices stained with Masson's trichrome in Tg-DN-Mst1, *Mst1*$^{-/-}$ *Beclin1*$^{+/-}$ *Beclin1*$^{+/-}$ -Tg-DN-Mst1, and NTg mice after 6 weeks of MI are shown. (**e**) Echocardiographic analyses were conducted after 6 weeks of MI. *Left:* Comparison of fractional shortening (%FS) in Tg-DN-Mst1, *Mst1*$^{-/-}$*Beclin1*$^{+/-}$*Beclin1*$^{+/-}$ -Tg-DN-Mst1, and NTg mice. Data are reported as mean ± SEM. * $P < 0.05$ vs NTg mice after 6-week MI. *Right:* Representative images of echocardiographs of Tg-DN-Mst1, *Mst1*$^{-/-}$*Beclin1*$^{+/-}$ *Beclin1*$^{+/-}$-Tg-DN-Mst1, and NTg mice 6 weeks after coronary artery ligation are shown.

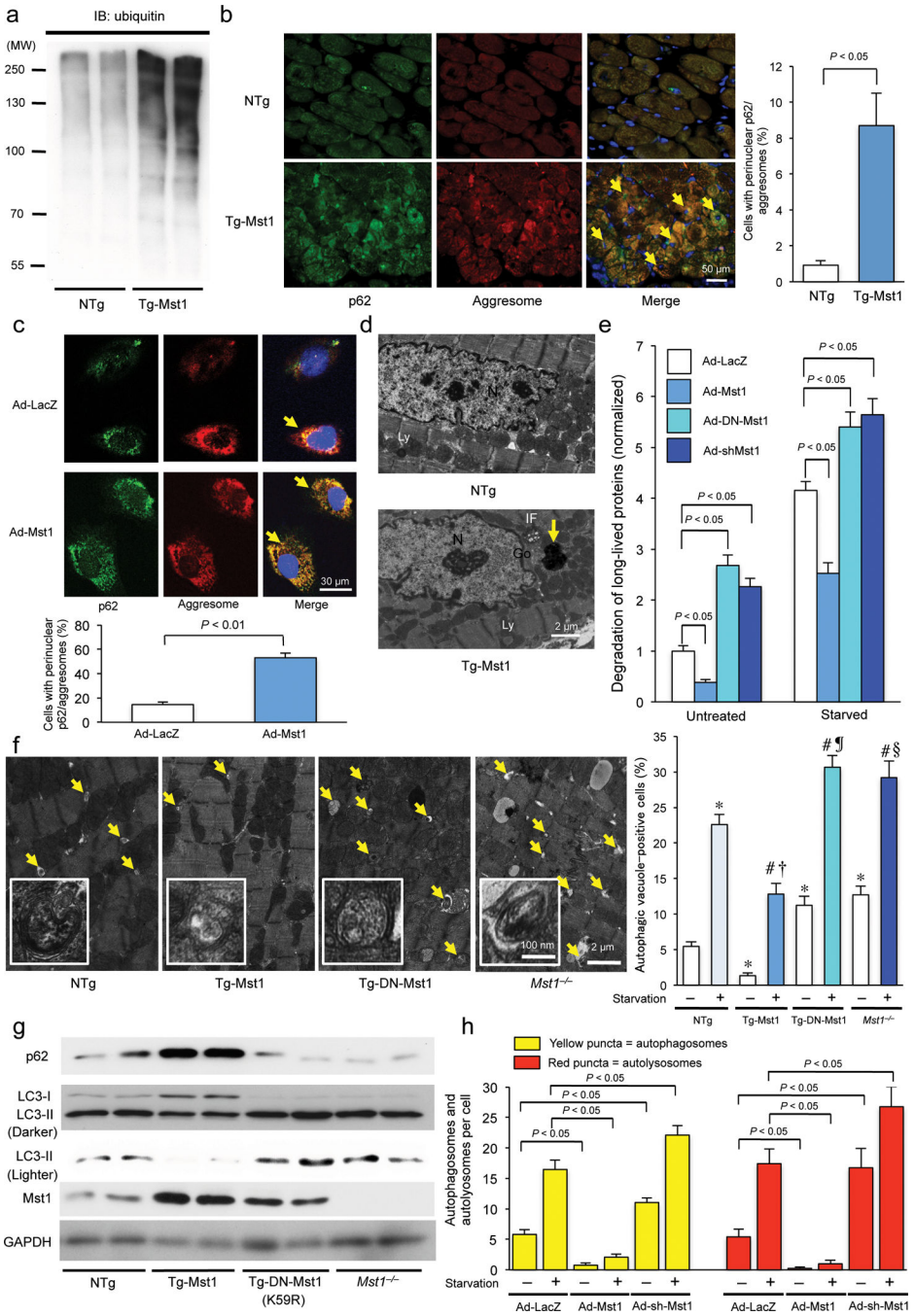

Figure 2. Mst1 promotes accumulation of protein aggresomes and p62/SQSTM1 and inhibits autophagy in cardiomyocytes

(**a**) Immunoblot analysis of heart homogenates with ubiquitin-specific antibody. Results represent means from 3 independent experiments. (**b**) *Left:* Representative immunofluorescent images of staining with p62/SQSTM1 (green), DAPI (blue), and ProteoStat® aggresome detection reagent (red), a marker of protein aggregation, in NTg and Tg-Mst1 hearts are shown. *Right:* The number of cells with aggresomes co-localized with p62/SQSTM1 in cardiomyocytes, indicated by yellow color in the merged images (arrows),

was counted (n = 5 in each group). Data are reported as mean ± SEM. (**c**) *Upper:* Representative immunofluorescent images of staining with p62/SQSTM1 (green), DAPI (blue), and ProteoStat® aggresome detection reagent (red) in Ad-LacZ-transduced and Ad-Mst1-transduced cultured cardiomyocytes are shown. *Lower:* The number of CMs with aggresomes co-localized with p62/SQSTM1, indicated by yellow color in the merged images (arrows), was counted (n = 6 in each group). Data are reported as mean ± SEM. (**d**) Representative images of aggresomes detected by transmission electron microscopy in NTg and Tg-Mst1 hearts. The aggresomes (arrow), embedded in a dense meshwork of intermediate filaments (IF) adjacent to the Golgi apparatus (Go), appeared as electron dense amorphous objects. N: Nucleus, Ly: Lysosome. Results represent means from 4 independent experiments. (**e**) Long-lived protein degradation assay. Quantitative analysis of the degradation rate of long-lived proteins, as indicated by the ratio of the TCA-soluble medium to TCA-precipitated cell lysate ^{3}H-l-valine radioactivity, is shown (n = 3 in each group). Data are reported as mean ± SEM. (**f**) *Left:* Representative images of autophagosomes (arrows and insets) detected by transmission electron microscopy after 48 hours of starvation in Tg-Mst1, Tg-DN-Mst1, *Mst1*$^{-/-}$, and NTg hearts are shown. *Right:* Quantitative analysis of the number of autophagosomes is shown (n = 3 in each group). Data are reported as mean ± SEM. * P < 0.05 vs NTg - Baseline; # P < 0.05 vs NTg - starvation; † P < 0.05 vs Tg-Mst1 - Baseline; ¶ P < 0.05 vs Tg-DN-Mst1 - Baseline; § P < 0.05 vs *Mst1*$^{-/-}$ - Baseline. (**g**) Representative immunoblot images of heart homogenates with antibodies to p62/SQSTM1, LC3, Mst1, and GAPDH are shown. Results represent means from 3 independent experiments. (**h**) Cardiomyocytes were transduced with Ad-Mst1, Ad-shMst1, or Ad-LacZ 24 hours after Ad-mRFP-GFP-LC3 transduction and treated with glucose-free media. The mean numbers of autophagosomes, represented by yellow puncta in merged images, and autolysosomes, represented by red puncta in merged images, per cell are shown (n = 3 in each group). Data are reported as mean ± SEM. * P < 0.05 vs Ad-LacZ/GD(−); # P < 0.05 vs Ad-LacZ/GD(+). Representative images of fluorescent LC3 puncta after Ad-mRFP-GFP-LC3 transduction are shown in Supplementary Figure 2e.

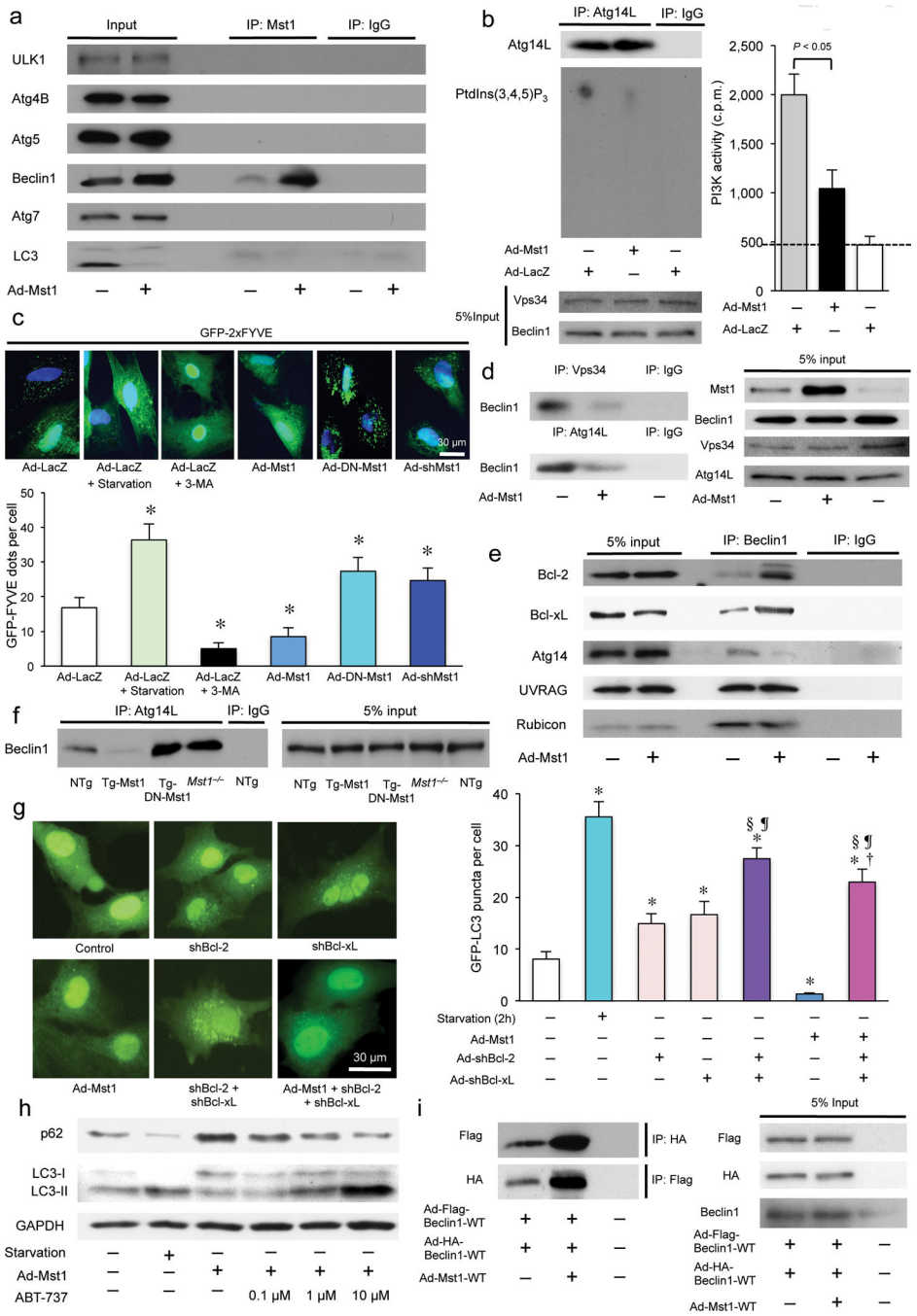

Figure 3. Mst1 physically interacts with Beclin1 and enhances its binding with Bcl-2/Bcl-xL, thereby inhibiting the kinase activity of the Beclin1-Vps34 (Class III PI3K) complex through modulation of the Atg14L-Beclin1 interaction and Beclin1 homodimerization in CMs

(**a**) Cardiomyocytes were transduced with or without Ad-Mst1. Forty-eight hours after transduction, lysates were extracted for immunoprecipitation with Mst1-specific antibody or control IgG, followed by probing with ULK1, Atg4B, Atg5, Beclin1, Atg7, or LC3 antibody. Representative images are shown. Results represent means from 3 independent experiments. (**b**) Lipid kinase assay of Beclin1-Vps34 complex. Cardiomyocytes were transduced with Ad-Mst1 or Ad-LacZ. *Left:* Endogenous Vps34 complex was

immunoprecipitated using Atg14L-specific antibody for the *in vitro* kinase assay. The resulting radioactive phosphatidylinositol 3-phosphate (PtdIns(3,4,5)P_3), a reaction product, was separated by TLC. *Right:* Radioactive PtdIns(3,4,5)P_3 was excised from thin layer plates and the radioactivity was measured in an LSC (n = 4 in each group). Data are reported as mean ± SEM. (**c**) Membrane-associated phosphoinositide 3-kinase (PI3K) assay *in situ*. Cardiomyocytes were transduced with Ad-Mst1, Ad-DN-Mst1, Ad-sh-Mst1, or Ad-LacZ 24 hours after Ad-GFP-2xFYVE transduction and then treated with or without 3-MA (5 mM) or glucose deprivation for 2 hours. *Upper:* Representative images of GFP-2xFYVE dots are shown. *Lower:* Quantitative analysis of the number of GFP-2xFYVE dots is shown (n = 6 in each group). Data are reported as mean ± SEM. * $P < 0.05$ vs Ad-LacZ, starvation (−). (**d**) Cardiomyocytes were transduced with Ad-Mst1 or Ad-LacZ. Forty-eight hours after transduction, lysates were extracted for immunoprecipitation with Atg14L-specific antibody, Vps34-specific antibody or control IgG, followed by probing with Beclin1-specific antibody. (**e**) Cardiomyocytes were transduced with or without Ad-Mst1. Forty-eight hours after transduction, lysates were extracted for immunoprecipitation with Beclin1 antibody or control IgG, followed by probing with antibodies to Bcl-2, Bcl-xL, Atg14, UVRAG, or Rubicon. Representative images are shown. Results represent means from 3 independent experiments. (**f**) Heart homogenates obtained from NTg, Tg-Mst1, Tg-DN-Mst1, or *Mst1*$^{-/-}$ mice were immunoprecipitated with Atg14L antibody or control IgG, followed by probing with Beclin1 antibody. Representative images are shown. Results represent means from 3 independent experiments. (**g**) Cardiomyocytes were transduced with Ad-GFP-LC3 with or without Ad-Mst1 either in the absence or presence of Ad-sh-Bcl-2 or Ad-sh-Bcl-xL. *Left:* Representative images of GFP-LC3 puncta are shown. *Right:* Quantitative analysis of the number of GFP-LC3 puncta is shown (n = 6 in each group). Data are reported as mean ± SEM. * $P < 0.05$ vs untreated control; † $P < 0.05$ vs Ad-Mst1; § $P < 0.05$ vs Ad-shBcl-2; ¶ $P < 0.05$ vs Ad-shBcl-xL. (**h**) Cardiomyocytes transduced with or without Ad-Mst1 were treated with ABT-737 (0, 0.1, 1, 10 μM) for 12 hours. Representative immunoblots with antibodies to p62/SQSTM1, LC3 and GAPDH are shown. Results represent means from 3 independent experiments. (**i**) An assay for Beclin1 dimerization. Cardiomyocytes were transduced with Ad-3xFlag-Beclin1-WT and Ad-3xHA-Beclin1-WT with or without Ad-Mst1. Forty-eight hours after transduction, lysates were extracted for immunoprecipitation with HA-specific or Flag-specific antibody, followed by probing with Flag-specific or HA-specific antibody, respectively. Representative images are shown. Results represent means from 3 independent experiments.

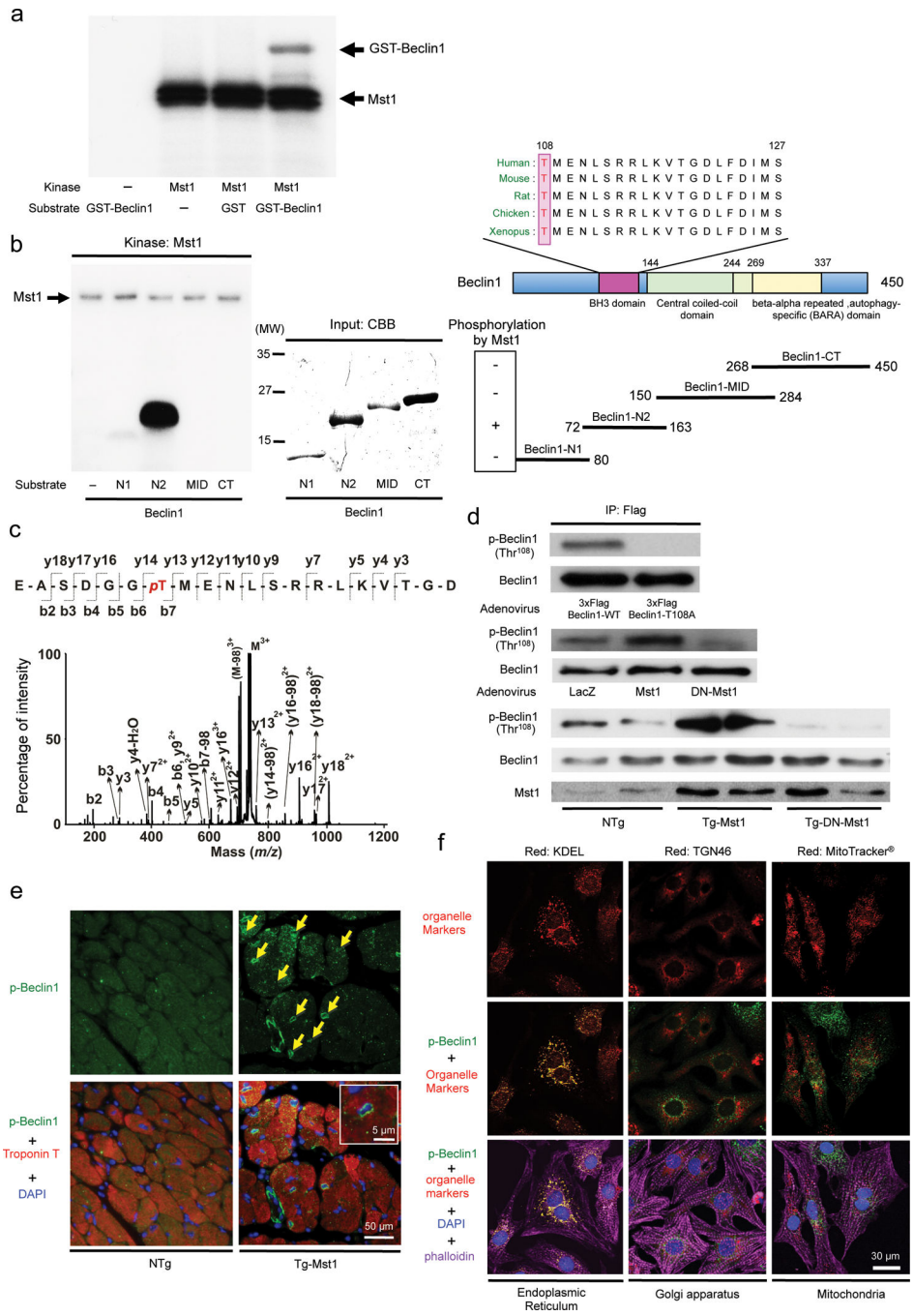

Figure 4. Mst1 phosphorylates Beclin1 at Thr^{108}, located in its BH3 domain

(**a**) *In vitro* kinase assays were carried out by incubating recombinant GST-Beclin1-WT protein with recombinant Mst1 in the presence of ^{32}P-labeled ATP. Reactions were analyzed by SDS-PAGE followed by autoradiography. Representative images are shown. Results represent means from 3 independent experiments. (**b**) The indicated recombinant partial proteins of Beclin1 were incubated with recombinant Mst1 in the presence of ^{32}P-labeled ATP for *in vitro* kinase assays. Representative images are shown. Results represent means from 3 independent experiments. (**c**) The MS/MS spectrum of the Beclin1-NT2 peptide

[102–121]. The peptide treated with Mst1 contained a phosphorylated Thr^{108}. (**d**) *Upper:* Cardiomyocytes were transduced with wild-type 3x Flag-tagged Beclin1 or T108A mutant. Ectopically expressed Beclin1 proteins were immunoprecipitated with a Flag-M2 antibody and detected with an antibody against either Beclin1 phosphorylated at Thr^{108} or total Beclin1. *Middle:* Cardiomyocytes were transduced with Ad-Mst1, Ad-DN-Mst1, or Ad-LacZ. Expression and phosphorylation of Beclin1 was examined by immunoblots with specific antibodies. Phospho-Beclin1 (Thr^{108}) antibody detects Beclin1 phosphorylated by Mst1. *Lower:* Immunoblot analysis of heart homogenates with phospho-Beclin1 (Thr^{108})-specific antibody. Representative images are shown. Results represent means from 3 independent experiments. (**e**) Representative immunofluorescent images of staining with phospho-Beclin1 (Thr^{108})-specific antibody (green), DAPI (blue), and Troponin T (red), a cardiac-specific marker, in NTg and Tg-Mst1 hearts are shown. Arrows indicate positive staining of phospho-Beclin1 (Thr^{108}) in the perinuclear region. Magnification of a perinuclear region is shown in the inset. Results represent means from 4 independent experiments. (**f**) Representative immunofluorescent images of staining with phospho-Beclin1 (Thr^{108})-specific antibody labeled with Alexa Fluor® 488 (green), DAPI (blue), Alexa Fluor® 555 phalloidin (violet), and either KDEL-specific antibody labeled with Alexa Fluor® 647 (red, a marker of endoplasmic reticulum), TGN46-specific antibody labeled with Alexa Fluor® 647 (red, a marker of golgi apparatus), or MitoTracker® Deep Red FM (red, a marker of mitochondria) in Ad-shScramble-transduced cardiomyocytes are shown. Results represent means from 4 independent experiments.

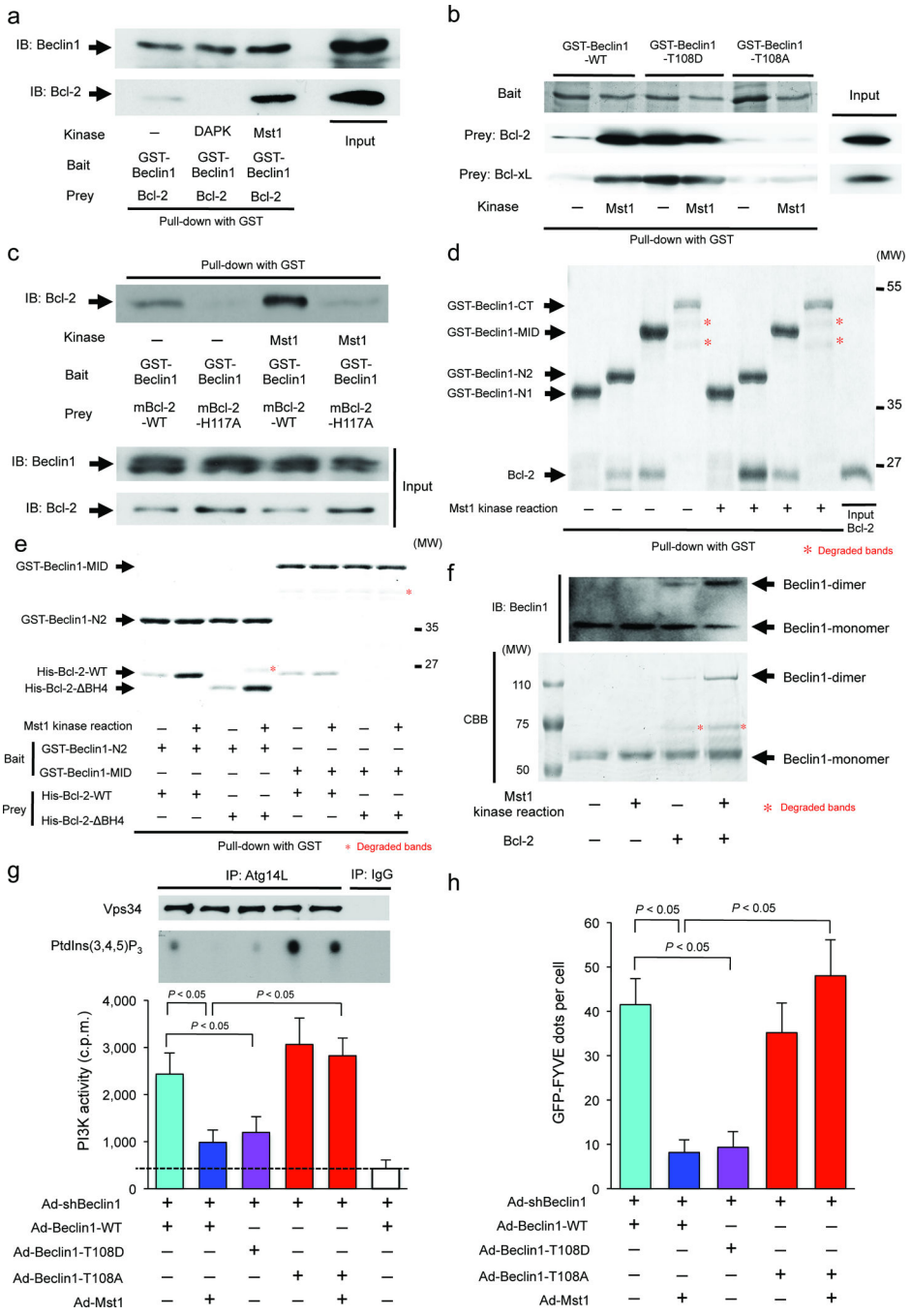

Figure 5. Beclin1 phosphorylated by Mst1 at Thr^{108} can interact with Bcl-2 family proteins, thereby inhibiting autophagy

(**a-f**) Pull-down assays after kinase reaction. (**a**) GST-Beclin1-WT was incubated with either Mst1 or death-associated protein kinase (DAPK) in the presence of ATP, and then incubated with a recombinant Bcl-2 protein to conduct pull-down assays. (**b**) GST-Beclin1-WT, GST-Beclin1-T108D, or GST-Beclin1-T108A was incubated with or without Mst1 in the presence of ATP, and then incubated with either Bcl-2 or Bcl-xL protein. (**c**) GST-Beclin1-WT was incubated with or without Mst1 in the presence of ATP, and then incubated with

Bcl-2-WT or Bcl-2-H117A proteins. (**d**) The indicated recombinant GST-tagged partial proteins of Beclin1 were incubated with or without Mst1 in the presence of ATP, and then incubated with Bcl-2 protein. (**e**) GST-Beclin1-N2 or GST-Beclin1-MID was incubated with or without Mst1 in the presence of ATP, and then incubated with either His-Bcl-2-WT or His-Bcl-2-ΔBH4 proteins. (**f**) Non-tagged Beclin1-WT after kinase reaction with or without Mst1, cross-linked with or without Bcl-2, were separated by Native-PAGE. The gels were then visualized by both immunoblotting (*Upper*) and Coomassie Brilliant Blue staining (*Lower*). In (a) to (f), Representative images are shown. Results represent means from 3 independent experiments. (**g**) Lipid kinase assay of the Beclin1-Vps34 complex I. Cardiomyocytes were co-transduced with Ad-Beclin1-WT, Ad-Beclin1-T108A, or Ad-Beclin1-T108D either in the absence or presence of Ad-Mst1. *Upper:* Endogenous Vps34 complex was immunoprecipitated with Atg14L-specific antibody for the *in vitro* kinase assay. The resulting radioactive PtdIns(3,4,5)P_3 was separated by TLC. *Lower:* Radioactive PtdIns(3,4,5)P_3 was excised from thin layer plates and the radioactivity was measured in an LSC (n = 4, respectively). Data are reported as mean ± SEM. (**h**) Membrane-associated PI3K assay *in situ*. Cardiomyocytes were co-transduced with Ad-Beclin1-WT, Ad-Beclin1-T108A, or Ad-Beclin1-T108D in the absence or presence of Ad-Mst1 24 hours after Ad-GFP-2xFYVE transduction. Quantitative analysis of the number of GFP-2xFYVE dots is shown (n = 6 in each group). Data are reported as mean ± SEM.

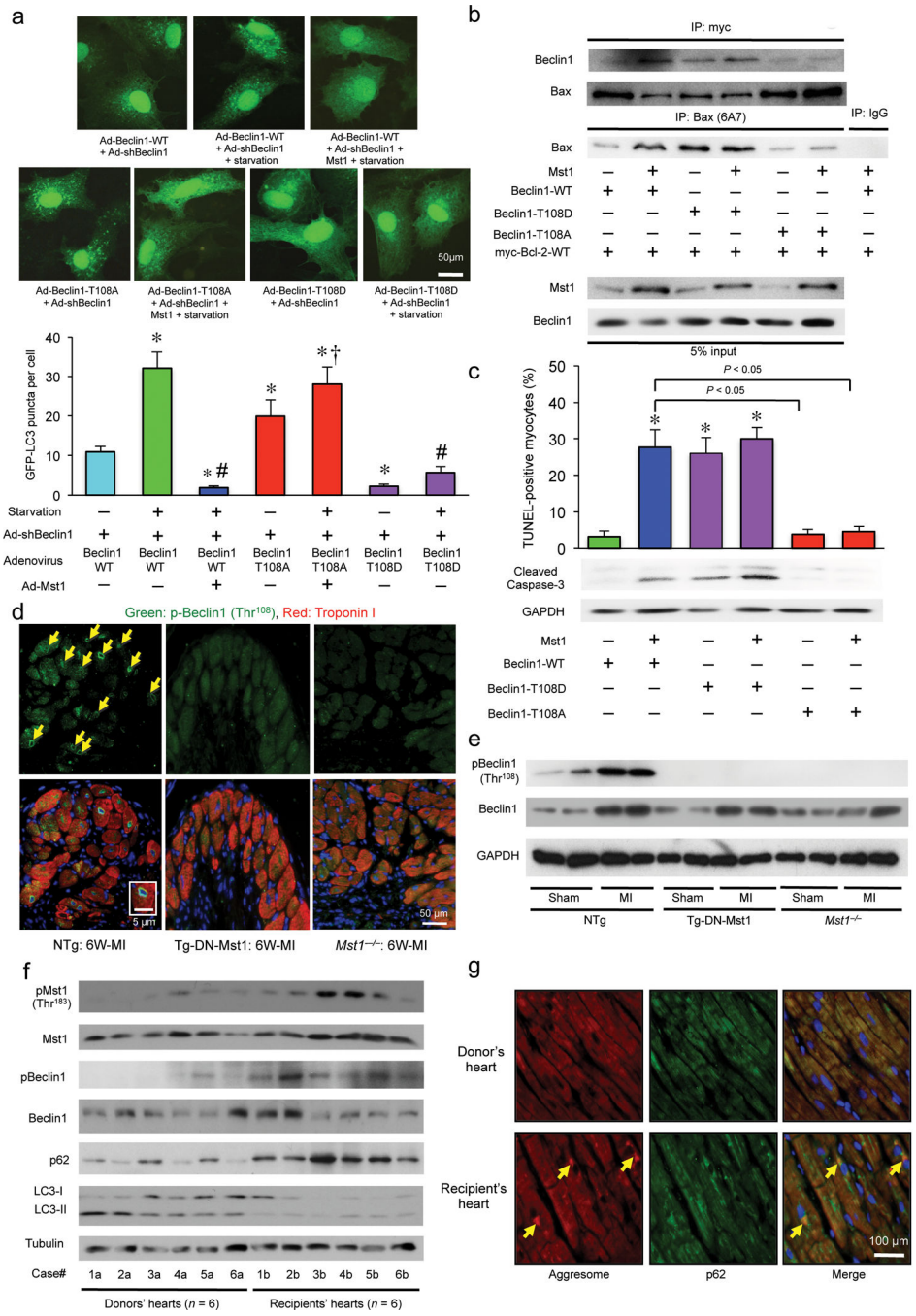

Figure 6. Mst1-induced phosphorylation of Beclin1 inhibits autophagy and induces apoptosis by sequestering Bcl-2 from Bax, thereby causing deterioration of cardiac function in failing hearts

(**a**) Cardiomyocytes were transduced with Ad-sh-Beclin1 and either Ad-Beclin1-WT, Ad-Beclin1-T108A, or Ad-Beclin1-T108D in the absence or presence of Ad-Mst1 24 hours after Ad-GFP-LC3 transduction, under either nutrient rich or starvation conditions. *Upper:* Representative images of GFP-LC3 puncta are shown. *Lower:* Quantitative analysis of the number of GFP-LC3 puncta is shown (n = 6 in each group). Data are reported as mean ± SEM. * $P < 0.05$ vs Ad-3xFlag-Beclin1-WT, Starvation (−), # $P < 0.05$ vs Ad-3xFlag-

Beclin1-WT, Starvation (+), † $P < 0.05$ vs Ad-3xFlag-Beclin1-WT+Ad-Mst1, Starvation (+). (**b**) Cardiomyocytes were transduced with Ad-myc-Bcl-2-WT either in the absence or presence of Ad-Mst1, and Ad-Beclin1-WT, Ad-Beclin1-T108D or Ad-Beclin1-T108A. Forty-eight hours after transduction, lysates were extracted for immunoprecipitation with antibodies to myc or Bax (clone 6A7), which recognizes only the activated form of Bax, followed by probing with Beclin1 or Bax antibodies. (**c**) Cardiomyocytes were transduced with or without Ad-Mst1 either in the absence or presence of Ad-Beclin1-WT, Ad-Beclin1-T108D or Ad-Beclin1-T108A. Quantitative analysis of the number of TUNEL-positive myocytes and immunoblot analysis of cardiomyocytes with cleaved caspase-3 antibody are shown ($n = 3$ in each group). Data are reported as mean ± SEM. * $P < 0.05$ vs Ad-Beclin1-WT, Ad-Mst1 (−). (**d**) Representative immunofluorescent images of staining with phospho-Beclin1 (Thr^{108})-specific antibody (green), DAPI (blue), and Troponin T antibody (red) in NTg, Tg-DN-Mst1 and $Mst1^{-/-}$ mice 6 weeks after coronary artery ligation are shown. Arrows and inset indicate positive staining of phospho-Beclin1 (Thr^{108}) in the perinuclear region. Results represent means from 4 independent experiments. (**e**) Immunoblot analysis of heart homogenates in Tg-DN-Mst1, $Mst1^{-/-}$, and NTg mice after 6 weeks of MI with phospho-Beclin1 (Thr^{108}), total Beclin1, and GAPDH antibodies. Representative images are shown. Results represent means from 3 independent experiments. (**f**) Immunoblot analyses of myocardial tissue homogenates from explanted hearts with antibodies to phospho-Mst1 (Thr^{183}), total Mst1, phospho-Beclin1 (Thr^{108}), total Beclin1, p62/SQSTM1, LC3, and tubulin are shown. Six samples (Case #1b - #6b) were from heart transplant recipients, and 6 samples (Case #1a - #6a) were from heart donors. Representative images are shown. Results represent means from 3 independent experiments. (**g**) Representative immunofluorescent images of staining with p62/SQSTM1 (green), DAPI (blue), and ProteoStat® aggresome detection reagent (red) in myocardial tissue samples from a heart transplant recipient (Case #1b) and donor (Case #1a) are shown. Yellow arrows indicate co-localization of aggresomes with p62 in the perinuclear region of CMs. Results represent means from 3 independent experiments.